INTERNATIONAL JOURNAL FOR NUMERICAL METHODS IN FLUIDS, VOL. 14, 631–664 (1992)

COMPUTATION OF TWO-DIMENSIONAL DAM-BREAK FLOOD FLOWS

JOHANNES VASSILIOU SOULIS

Division of Fluid Mechanics/Hydraulics, Department of Civil Engineering, Democrition University of Thrace, Xanthi 67100, Greece

SUMMARY

Sudden total collapse of a dam holding back a reservoir of water, whenever it occurs, becomes formidably impressive in the extent of destruction with which it is associated. The movement on a dry bed of a two-dimensional flood wave resulting from the break of a dam has been one of the most important and challenging subjects in rapidly varied unsteady flows from the computational point of view. An implicit time-marching finite volume numerical scheme was developed and subsequently applied for the solution of the two-dimensional unsteady open channel flow equations written in conservation form. In order to avoid the problems associated with a conventional grid system, a body-fitted non-orthogonal local co-ordinate system was utilized. The proposed numerical technique was applied to determine the stage hydrographs, water surface profiles and velocities of flood flows resulting from suddenly breached storage dams. Predictions were compared with an analytical solution, with available numerical solutions using MacCormack's two-step explicit scheme and with experimental measurements. Agreement between predictions and measurements regarding the wave front advancement and stage hydrographs is considered to be satisfactory.

KEY WORDS Unsteady 2D flow Dam-break flood waves Body-fitted co-ordinates Implicit scheme

1. INTRODUCTION

In recent years significant numerical method advances and computer-based algorithms have been made in fluid flow problems. These advances have provided engineers and scientists with the most powerful means of solving complex fluid-engineering problems. Sudden total collapse of a dam holding back a reservoir of water, whenever it occurs, becomes formidably impressive in the extent of destruction with which it is associated. The movement on a dry bed of a two-dimensional flood wave resulting from the break of a dam has been one of the most important and challenging subjects in rapidly varied unsteady flows from the computational point of view. Essentially, the flow properties are assumed to be invariant along the vertical direction. These simplified representations of a three-dimensional flow are justified where turbulent mixing, due to bottom roughness, effectively generates a uniform velocity distribution over the flow field. The associated flow problem has been the subject of extensive research work for the last 20 years. The governing flow equations for the two-dimensional shallow water flow were solved using the method of characteristics, the explicit finite difference method, the implicit finite difference method and the finite element method. Unlike one-dimensional flow, applications of two-dimensional unsteady flow are few in number and have only recently been appearing in the general literature. The basic flow equations are hyperbolic-type partial differential equations.

0271–2091/92/060631–34$17.00
© 1992 by John Wiley & Sons, Ltd.
Received January 1991
Revised June 1991

From the analysis of dam-break flood wave movement, two main difficulties arise which require specific consideration: (a) the proper mathematical formulation of the wave front region, especially for the period immediately after the dam-break when local accelerations are very high and the water surface slopes are exceedingly steep; (b) the proper satisfaction of the solid boundary conditions of a geometrically complex channel.

Xanthopoulos and Koutitas[1] numerically investigated the propagation of a flood wave on a two-dimensional dry plain. The velocity components, the water depth and the position of the water front for each time step were computed through an explicit finite difference scheme in Eulerian space. The forcing function consisted of the charge by a discharge hydrograph on a boundary point. The method was applied on a Northern Hellenic plain for the study of its inundation due to failure of an operating earth dam. However, the assumptions made about the governing flow equations restricted the possible applications of their model. Gallati *et al.*[2] presented a mathematical finite difference model solving the two-dimensional shallow water equations without the convective terms. The model showed good behaviour and the obtained results were close to the available data.

Townson and Al-Salihi[3] applied the method of characteristics to the quasi-2D shallow water equations written in cylindrical co-ordinates (radial flow, R–T space). Instant failure of a dam between walls which either converge or diverge was simulated. Comparisons were made with Ritter and Stoker solutions for parallel walls and different downstream depths. Physical model test results confirm general expectations that converging walls create deeper and faster flows downstream and vice versa. Katopodes and Strelkoff[4] developed a mathematical model of the two-dimensional dam-break flood wave based on the method of characteristics. The selection of the method was based on the fact that the curvilinear wave boundaries and irregular geometry associated with the dam-break problem in two space dimensions were poorly modelled by finite differences. However, secondary shock waves were not accounted for by the method. No comparisons with measured data were reported. A simple experiment was set up in order to establish the qualitative similarity with the mathematical model.

Popovska[5] developed a numerical model for two-dimensional unsteady flow in open channels using a simple time-split explicit scheme over the conservative form of the basic equations. The mathematically simulated wave front propagates 25% slower than the measured one, with an elongated form in the predominant flow direction. It was stated that the errors should not be attributed to the mathematical model only since the values of the physical model may be in error too. More investigation was therefore needed. Rajar and Cetina[6] solved the two-dimensional dynamic and continuity equations written in a curvilinear orthogonal co-ordinate system where one of the axes was aligned along assumed streamlines. The basic numerical procedure was taken from the well-known Patankar numerical method, but some new features had to be introduced. Measured and computed results showed surprisingly good agreement.

Dammuller *et al.*[7] analysed the unsteady flow in a curved channel. The equations describing the conservation of mass and momentum were transformed from a Cartesian co-ordinate system to a channel co-ordinate system. Then the equations were integrated over the depth to obtain a set of depth-averaged two-dimensional equations that were then solved using the MacCormack explicit finite difference scheme. They concluded that the agreement between computed and measured water levels was satisfactory. The computed wave speed is slower than the measured wave speed when the flow is near critical conditions. Bellos *et al.*[8] numerically examined the flood waves resulting from the instantaneous break of dams. The governing system of differential equations was transformed into an equivalent system applied over a square grid network in order to overcome the difficulties and inaccuracies associated with the determination of flow characteristics near the flow boundaries. It must be noted that a similar approach is adopted for the

current method. However, Bellos *et al.*[9] and Bellos[10] utilized the MacCormack two-step predictor–corrector explicit numerical scheme. Comparisons between computed and measured data showed satisfactory agreement. The MacCormack explicit time-splitting scheme was utilized by Garcia and Kawahita[11] for the development of a two-dimensional hydraulic simulation model that solves the St. Venant equations. The method has been found to be computationally efficient and warrants further development. However, the reported applications showed that the technique was not capable of accurately describing flow fields with irregular geometries owing to the rectangular grid used. Fennema and Chaudhry[12] utilized the Beam–Warming implicit finite difference scheme to integrate the equations describing two-dimensional unsteady free surface flows.

Katopodes and Wu[13] presented a finite element method of fourth-order accuracy. The method was explicit in time and was well suited for discontinuous flows. Samuels[14] examined two-dimensional (in plan) models over a flood plain using finite elements. Three different sets of model equations were introduced and their mathematical type and appropriate boundary conditions were discussed. Finally, Di Monaco and Molinaro[15] derived a finite element two-dimensional model of free surface flow. The verification was made against experimental data for the problem of the emptying of a reservoir due to dam-breaking. They concluded that the choice of initial conditions greatly influenced the accuracy and convergence of the solution, at least in the initial time steps.

This paper is an extension and improvement of previous research work on steady two-dimensional subcritical–supercritical flow for open channel calculations developed by Soulis and Bellos.[16] The general technique used is a combination of the finite element and finite difference metods. First, a transformation is introduced through which quadrilaterals in the physical domain are mapped into squares in the computational domain. The governing system of equations is thus transformed into an equivalent system applied over a square grid network. In the second phase a time-marching method is employed for the solution of the transformed system of equations. This scheme is well suited for flow computations where discontinuities of the flow may be present.

In order to validate the proposed numerical method, it was decided to test it against available experimental data[10] as well as availabe two-dimensional numerical solution results.[9] The two-dimensional algorithm was also used to simulate one-dimensional dam-break analytical[17]–numerical[18] solutions as well as experimental data.[19] The programme can be applied on any given topography provided that the assumptions about the flow conditions are met.

2. THE GOVERNING UNSTEADY FLOW EQUATIONS

Under the assumptions of homogeneous 2D incompressible flow with hydrostatic pressure distribution over a cross-section with wind and Coriolis forces neglected, the equations which govern the flow resulting from the rupture of a dam are written in matrix form as

$$\mathbf{W}_t + \mathbf{F}_x + \mathbf{G}_y = \mathbf{D}, \tag{1}$$

where

$$\mathbf{W} = \begin{bmatrix} h \\ hu \\ hv \end{bmatrix}, \qquad \mathbf{F} = \begin{bmatrix} hu \\ hu^2 + gh^2/2 \\ huv \end{bmatrix},$$

$$\mathbf{G}=\begin{bmatrix} hv \\ huv \\ hv^2+gh^2/2 \end{bmatrix}, \qquad \mathbf{D}=\begin{bmatrix} 0 \\ gh(S_{0x}-S_{fx}) \\ gh(S_{0y}-S_{fy}) \end{bmatrix}. \tag{2}$$

The subscripts x, y and t have been used to denote partial derivatives. In the above system u is the average velocity component in the longitudinal (x) channel direction, v is the average velocity component in the transverse (y) channel direction, t is the time, h is the water depth, g is the acceleration due to gravity, S_{0x} is the channel slope in the x-direction ($=-\partial z_0/\partial x$, with z_0 the bottom elevation), S_{0y} is the channel slope in the y-direction ($=-\partial z_0/\partial y$), S_{fx} is the resistance slope in the x-direction, S_{fy} is the resistance slope in the y-direction, x is the distance along the channel and y is the distance along the transverse to the channel axis. The resistance slopes are evaluated usng the Manning relation. Thus

$$S_{fx}=n^2 u\sqrt{(u^2+v^2)}/h^{4/3}, \tag{3}$$

$$S_{fy}=n^2 v\sqrt{(u^2+v^2)}/h^{4/3}, \tag{4}$$

where n is the Manning roughness coefficient of flow. In equations (3) and (4) the water depth h also has the meaning of flow hydraulic radius R.

3. INITIAL AND BOUNDARY FLOW CONDITIONS

The problem must be closed with an appropriate description of the initial and boundary conditions. The unsteady flow region expands both upstream and downstream from the dam-site flow region. The current method does not keep track of the boundaries of the unsteady flow region. The boundary conditions at the furthest upstream and downstream ends of the flow field at any time are known.

3.1. Initial flow

The following relations have been taken as initial conditions for the dam-break problem.

Upstream from the dam-site

$$h(x, y, t_0)=h_1(x, y, t_0), \tag{5}$$

$$u(x, y, t_0)=0{\cdot}0, \tag{6}$$

$$v(x, y, t_0)=0{\cdot}0, \tag{7}$$

where the subscript zero denotes initial values. The water depth h_1 depends on the upstream bottom slope. Thus

$$h_1(x, y, t_0)=h_1(0{\cdot}0^-, y, t_0)+S_{0x}x, \tag{8}$$

where in this case x is the distace along the channel measured positive from the dam-site located at $x=0{\cdot}0^-$. The superscript minus denotes the distance immediately upstream from the dam-site.

At the dam-site (denoted by the subscript 1)

$$h(x_1, y_1, t_0)=\tfrac{4}{9}h_1(x_1, y_1, t_0), \tag{9}$$

$$u(x_1, y_1, t_0)=\sqrt{[gh(x_1, y_1, t_0)]}, \tag{10}$$

$$v(x_1, y_1, t_0)=0{\cdot}0. \tag{11}$$

The above equations represent the Ritter[20] solution for one-dimensional frictionless flow.

Downstream from the dam-site

$$h(x, y, t_0) = 0{\cdot}001 h_1, \tag{12}$$

$$u(x, y, t_0) = 0{\cdot}0, \tag{13}$$

$$v(x, y, t_0) = 0{\cdot}0. \tag{14}$$

The above equations represent the dry bed conditions. However, dry bed problems indicate that the flow depth at the wave tip reduces to zero while the tangent to the profile becomes vertical. Whenever one tries to solve the above problem numerically, one faces serious difficulties. To avoid these unfavourable consequences, all depths are set equal to a minimum value of the order of $0{\cdot}001h_1$. The same procedure is applied inversely at the trailing edge of the wave in case the flow depth at the upstream boundary reduces to zero. Numerical experimentation has shown that the above minimum value of $0{\cdot}001h_1$ was sufficiently small. Further reduction of this value did not alter the flow properties. Figure 1 shows a finite length reservoir on a sloping channel.

3.2. Upstream flow boundary

The flow regime obtaining at the upstream end of a reach determines the nature of the boundary conditions required there. For all current method applications one-dimensional flow is considered. With subcritical flow one physical condition is required. This condition requires that the flow normal to the upstream face must be zero. The other is then found by solving a difference equation based on the characteristic form of equations (1) for one-dimensional flow. The backward characteristic equation is given by[21]

$$(hu)_t + (u-c)(hu)_x - (u+c)[h_t + (u-c)h_x] = gh(S_{0x} - S_{fx}), \tag{15}$$

where

$$c = (gh)^{1/2} \tag{16}$$

is the celerity. The velocity u is considered to be zero and equation (15) is modified accordingly.

3.3. Downstream flow boundary

The flow regime obtaining at the downstream end of the reach is also considered to be one-dimensional. The flow quantities of depth and velocity can be calculated from the simultan-

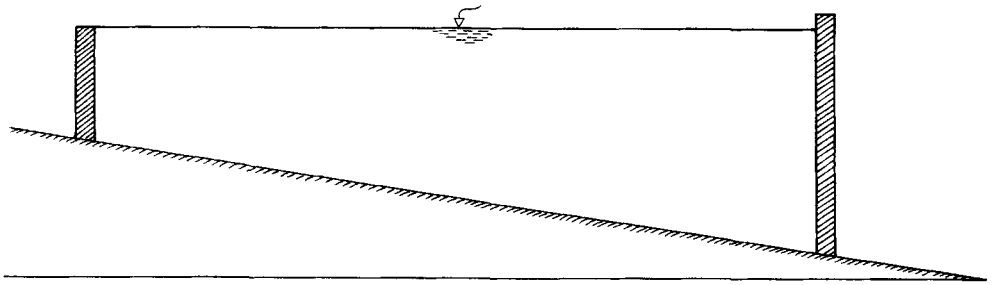

Figure 1. A finite length reservoir

eous solution of the two characteristic equations. These two equations comprise a linear algebraic system with unknowns h and u. In practice the water depth is calculated using equation (38) of Section 5.2, while the flow velocity is calculated within the main flow discretization routine, which is an iterative process.

3.4. Solid boundaries

The condition of no mass flow across the solid boundaries of the open channel needs to be applied. This condition requires the velocity component normal to the solid face, q_n, to be zero:

$$q_n = 0{\cdot}0. \tag{17}$$

4. TRANSFORMATION OF THE UNSTEADY FLOW EQUATIONS

In order to overcome the difficulties and inaccuracies associated with the determination of flow characteristics near the flow boundaries as well as to have the ability to use dense or sparse computational grid points in predefined flow regions of the tested area, the governing system of differential equations (1) is transformed into an equivalent system applied over a square grid network. Thus the essence of the present numerical scheme is that quadrilaterals in the physical domain will be separately mapped into squares, subsequently called finite volumes, in the computational domain by independent transformations from global (x, y) to local (ξ, η) co-ordinates as shown in Figure 2. The quadrilaterals are packed around the boundaries of the open channel and cover the whole flow field. This is shown in Figure 3. Figure 4 shows the computational grid which emerged as a result of the applied transformation. Linear shape functions are defined in terms of a non-orthogonal co-ordinate system ξ, η for the quadrilaterals (see Figure 2).

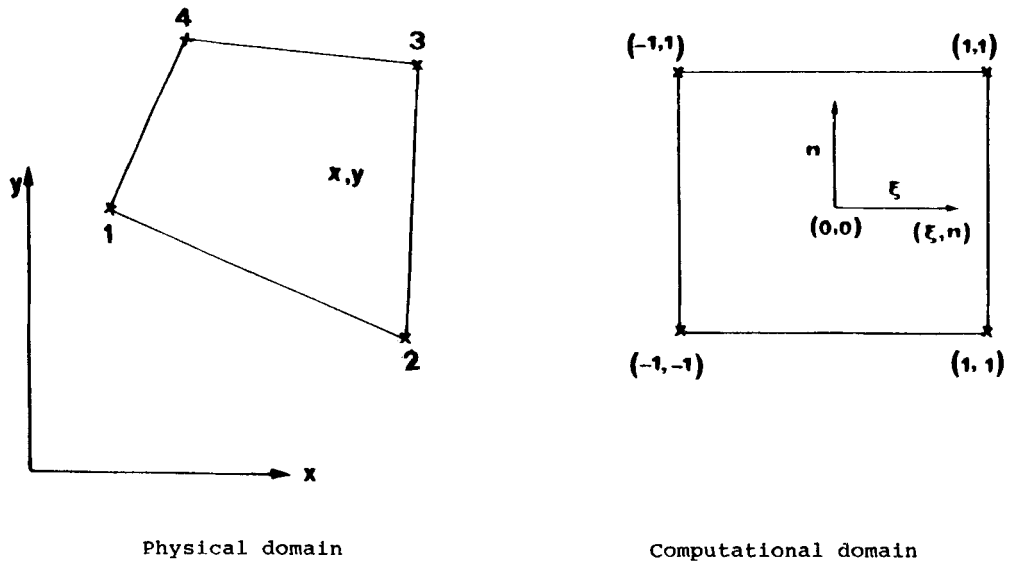

Figure 2. Quadrilaterals are mapped into squares

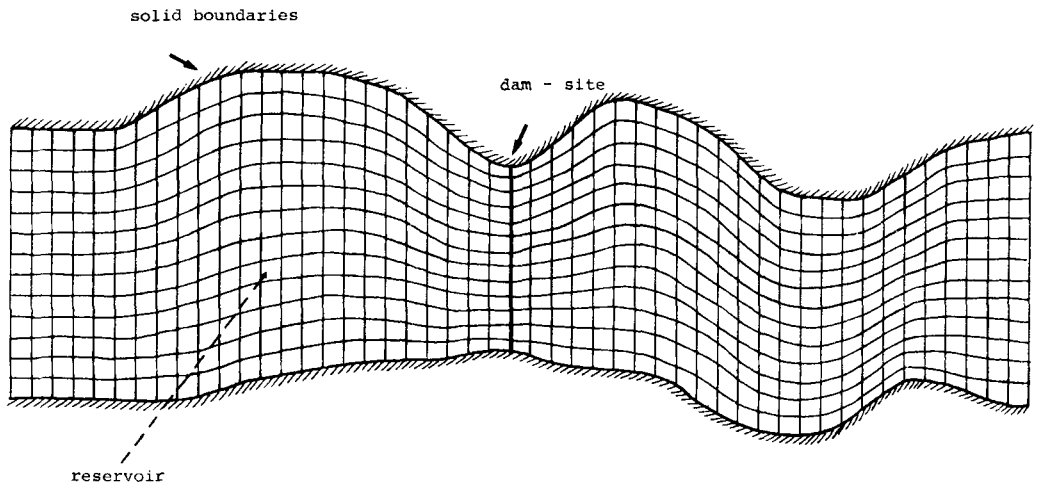

Figure 3. Typical grid (13 × 49)

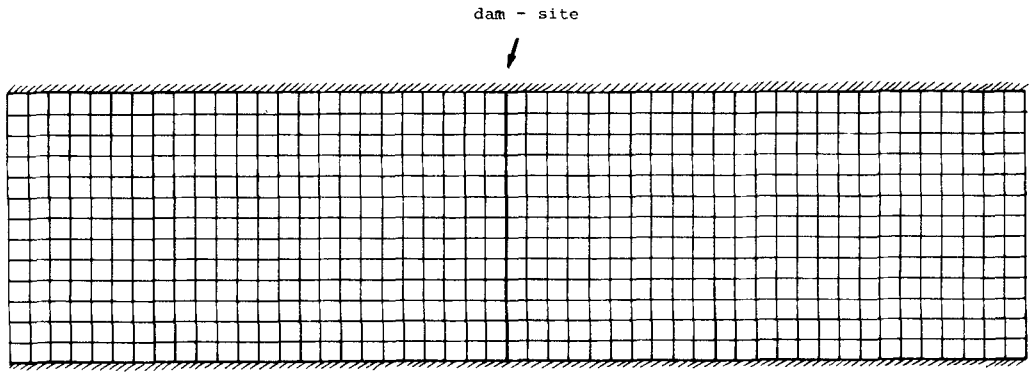

Figure 4. Transformed (computational) grid

Let **H** be the transformation matrix from the physical system to the computational system; then

$$\mathbf{H}=\begin{bmatrix} x_\xi & x_\eta \\ y_\xi & y_\eta \end{bmatrix}, \tag{18}$$

$$J^{-1}=[\mathbf{H}]. \tag{19}$$

The following relations hold:[22,23]

$$x_\xi = J^{-1}\eta_y, \qquad x_\eta = -J^{-1}\xi_y, \qquad y_\xi = -J^{-1}\eta_x, \qquad y_\eta = J^{-1}\xi_x. \tag{20}$$

Under the aforementioned transformation of equations (1) into the local co-ordinate system ξ, η

they assume the form

$$\mathbf{W}'_t+\mathbf{F}'_\xi+\mathbf{G}'_\eta=\mathbf{D}', \tag{21}$$

$$\mathbf{W}'=J^{-1}\begin{bmatrix} h \\ hu \\ hv \end{bmatrix}, \qquad \mathbf{F}'=J^{-1}\begin{bmatrix} hU \\ hUu+\xi_x gh^2/2 \\ hUv+\xi_y gh^2/2 \end{bmatrix},$$

$$\mathbf{G}'=J^{-1}\begin{bmatrix} hV \\ hVu+\eta_x gh^2/2 \\ hVv+\eta_y gh^2/2 \end{bmatrix}, \quad \mathbf{D}'=J^{-1}\begin{bmatrix} 0 \\ gh(S_{0x}-S_{fx}) \\ gh(S_{0y}-S_{fy}) \end{bmatrix}, \tag{22}$$

U and V being the velocity components in the local co-ordinate system. The velocities u and v are related to U and V by

$$\begin{bmatrix} u \\ v \end{bmatrix}=\mathbf{H}\begin{bmatrix} U \\ V \end{bmatrix}. \tag{23}$$

5. NUMERICAL SOLUTION PROCEDURE

5.1. Main flow discretization

The unsteady flow equations (21) may be written in conservation form for a control volume of unit height (see Figure 5) and a time step Δt as

$$-\Delta(J^{-1}h)=[\Delta(J^{-1}hU)\Delta\eta+\Delta(J^{-1}hV)\Delta\xi]\Delta t/\Delta\xi\Delta\eta \quad \text{(continuity)}, \tag{24}$$

$$-\Delta(J^{-1}hu)=\{\Delta[J^{-1}(hUu+\xi_x gh^2/2)]\Delta\eta+\Delta[J^{-1}(hVu+\eta_x gh^2/2)]\Delta\xi\}\Delta t/\Delta\xi\Delta\eta$$
$$-J^{-1}gh(S_{0x}-S_{fx})\Delta t \quad (x\text{-momentum}), \tag{25}$$

$$-\Delta(J^{-1}hv)=\{\Delta[J^{-1}(hUv+\xi_y gh^2/2)]\Delta\eta+\Delta[J^{-1}(hVv+\eta_y gh^2/2)]\Delta\xi\}\Delta t/\Delta\xi\Delta\eta$$
$$-J^{-1}gh(S_{0y}-S_{fy})\Delta t \quad (y\text{-momentum}). \tag{26}$$

The notation of the general flux balancing across the finite volume is also shown in Figure 5. Three cases are involved.

For the mass flux an XFLUX at grid point (i, j) is defined as

$$(\text{XFLUX})_{i,j}=[(J^{-1}hU)_{i+1,j}+(J^{-1}hU)_{i,j})]\Delta\eta/2, \tag{27}$$

while the YFLUX at the same grid point is defined as

$$(\text{YFLUX})_{i,j}=[(J^{-1}hV)_{i,j}+(J^{-1}hV)_{i,j-1})]\Delta\xi/2. \tag{28}$$

For the x-momentum flux balance the corresponding $(\text{XFLUX})_{i,j}$ and $(\text{YFLUX})_{i,j}$ are defined as

$$(\text{XFLUX})_{i,j}=\{[J^{-1}(hUu+\xi_x gh^2/2)]_{i+1,j}+[J^{-1}(hUu+\xi_x gh^2/2]_{i,j}\}\Delta\eta/2, \tag{29}$$

$$(\text{YFLUX})_{i,j}=\{[J^{-1}(hVu+\eta_x gh^2/2)]_{i,j}+[J^{-1}(hVu+\eta_x gh^2/2]_{i,j-1}\}\Delta\xi/2. \tag{30}$$

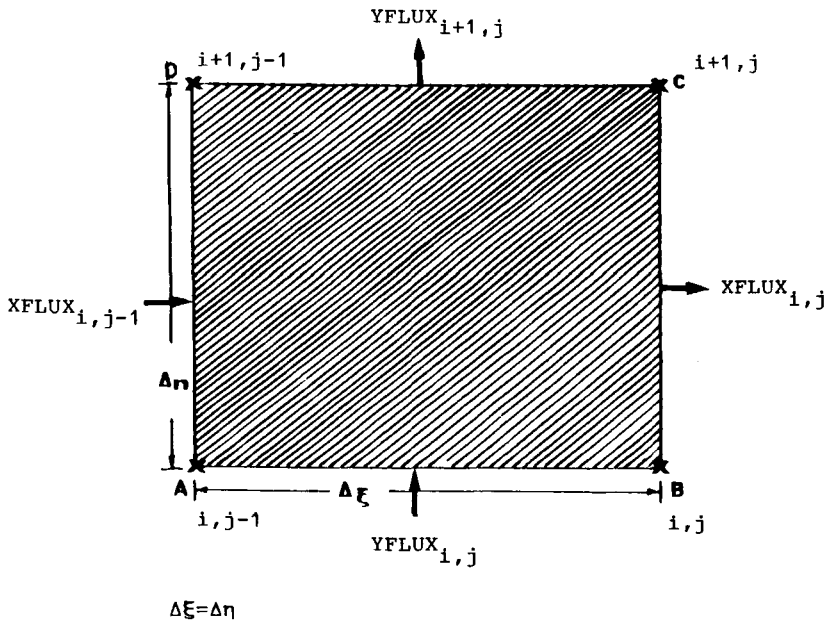

Figure 5. Notation for mass flux balancing across a finite volume

For the y-momentum flux balance the correspondng $(\mathrm{XFLUX})_{i,j}$ and $(\mathrm{YFLUX})_{i,j}$ are defined as

$$(\mathrm{XFLUX})_{i,j}=\{[J^{-1}(hUv+\xi_y gh^2/2)]_{i+1,j}+[J^{-1}(hUv+\xi_y gh^2/2]_{i,j}\}\Delta\eta/2, \tag{31}$$

$$(\mathrm{YFLUX})_{i,j}=\{[J^{-1}(hVv+\eta_y gh^2/2)]_{i,j}+[J^{-1}(hVv+\eta_y gh^2/2]_{i,j-1}\}\Delta\xi/2. \tag{32}$$

The terms $\Delta(J^{-1}hU)$ and $\Delta(J^{-1}hV)$ of the RHS of equation (24) are defined as

$$\Delta(J^{-1}hU)=(\mathrm{XFLUX})_{i,j}-(\mathrm{XFLUX})_{i,j-1}, \tag{33}$$

$$\Delta(J^{-1}hV)=(\mathrm{YFLUX})_{i+1,j}-(\mathrm{YFLUX})_{i,j}. \tag{34}$$

A similar approach is adopted for the RHS differences of equation (25) and (26).

5.2. *Boundary conditions*

Upstream end. At the beginning of the reach ($i=1, IM$ and $j=1$)

$$u_{i,1}^{(n+1)}=0{\cdot}0, \tag{35}$$

$$v_{i,1}^{(n+1)}=0{\cdot}0, \tag{36}$$

$$h_{i,1}^{(n+1)}=h_{i,1}^{(n)}+\lambda_{i,1}c_{i,1}^{(n)}(h_{i,2}^{(n)}-h_{i,1}^{(n)})-\lambda_{i,1}(hu)_{i,2}^{(n)}-gh_{i,1}^{(n)}(S_{0x}-S_{fx})_{i,1}^{(n)}\Delta t/c_{i,1}^{(n)}, \tag{37}$$

where $\lambda=\Delta t/\Delta x$ and the superscript $(n+1)$ denotes the current time step.

Downstream end. At the end of the reach ($i=1, 1M$ and $j=JM$) the following formula was found to be suitable:[24]

$$h_{i,JM}^{(n+1)}=h_{i,JM}^{(n)}-\lambda_{i,JM}[(hu)_{i,JM}^{(n)}-(hu)_{i,JM-1}^{(n)}]. \tag{38}$$

Solid surfaces. To this end, the fluxes hu and hv across the faces of the finite volume, which is bounded by the body surface, are calculated so as to satisfy equation (17). This is easily achieved in the local co-ordinate system ξ, η by requiring the velocity component V through the solid body of the structure to be zero, i.e. $V_{1,j}^{(n+1)}=0{\cdot}0$ for the 'lower' surface and $V_{IM,j}^{(n+1)}=0{\cdot}0$ for the 'upper' surface.

5.3. The iterative scheme

A simple implicit scheme was used for the numerical solution of the continuity equation (24), the x-momentum equation (25) and the y-momentum equation (26). The solution procedure starts with the initial flow conditions (5)–(14). At a given time step Δt the mass and momenta fluxes (27)–(32) are used to obtain the changes $\Delta(J^{-1}h)$, $\Delta(J^{-1}hu)$ and $\Delta(J^{-1}hv)$ and thus the values of h, u and v for the time step under consideration. Empasis must be given to the fact that these changes are not added to the previous pseudotime step in order to yield the current values of h, u and v. They are simply added to the previous time step solution (n). Thus the following equations hold:

$$h_{i,j}^{(n+1)}=h_{i,j}^{(n)}+\Delta(h)_{i,j}^{(n+1)}, \tag{39}$$

$$(hu)_{i,j}^{(n+1)}=(hu)_{i,j}^{(n)}+\Delta(hu)_{i,j}^{(n+1)}, \tag{40}$$

$$(hv)_{i,j}^{(n+1)}=(hv)_{i,j}^{(n)}+\Delta(hv)_{i,j}^{(n+1)}. \tag{41}$$

Of course, the boundary conditions, (35)–(38) need to be properly satisfied. Iterations were continued until the maximum change of u-velocity component between successive iterations dropped below 0·0001% over the average flow field velocity. At the same time a second convergence criterion was incorporated. This was based on the average over the flow field velocity component u. In this case the average change between successive iterations was required to drop below 0·000 0025%. Both criteria need to be satisfied simultaneous. The need to utilize and second criterion was due to local error instability. Once the solution is achieved, a new time step is incorporated and the current solution becomes the initial flow condition for the new time step. The total number of iterations required to achieve convergence was strongly dependent on the actual time. For the initial time steps this number was of the order of 30 or so, depending of course upon the geometrical complexity and the head difference between the reservoirs. However, a few time steps later, when the flow field is rather settled, the number of iterations required to achieve the above-mentioned convergence dropped to three or so. Thus the applied implicit scheme proved to be efficient in achieving the numerical solution. Grid reduction tests have shown that the grid size, i.e. the ratio of Δx to Δy, does not affect the accuracy of the soluton. However, in cases where this ratio becomes relatively high it does affect the solution convergence, and in extreme cases the solution breaks down. Then one has to apply moderate ratios in order to achieve convergence. Fortunately, the computational grid is easily formed, requiring minimal programming effort.

The time increment Δt in a numerical scheme is always subject to certain restrictions because of instability considerations. The theoretical maximum stable time step Δt is determined by the CFL criterion

$$\Delta t=\frac{\Delta x}{u+(gh)^{1/2}}. \tag{42}$$

In practice the above-calculated Δt was multiplied by a time factor so as to achieve smooth convergence. In order to speed up the solution, the value of the time factor was determined by

numerical experimentation. For a typical dam-break flow problem solution this value was found to be of the order of 0·1 when the h-value of equation (42) was the reservoir water depth furthest upstream.

The computational procedure was greatly facilitated by the simultaneous use of the physical

Table I

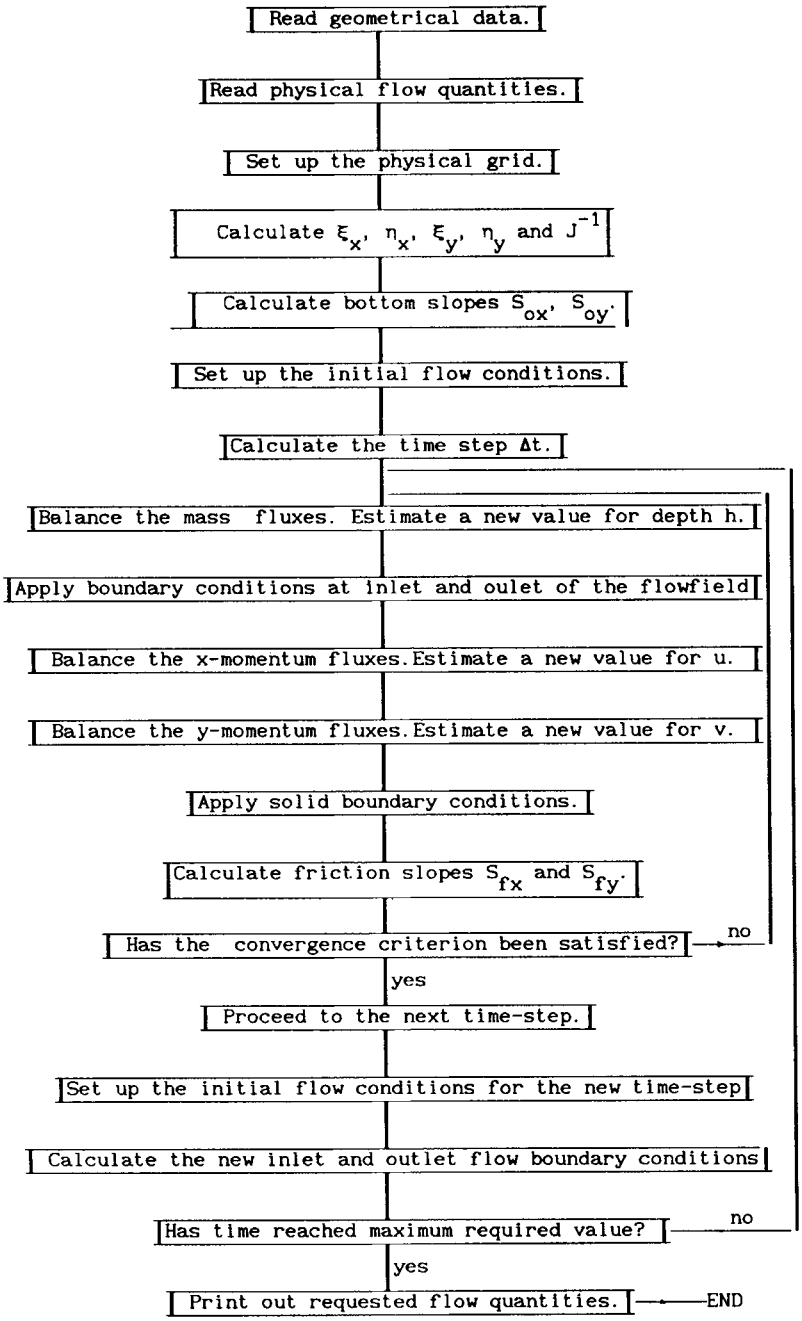

and computational planes. For instance, the utilization of the velocity components U and V in the computational grid enables the solid boundary conditions to be easily and accurately applied. At the same time the inlet and outlet flow field boundary conditions are applied using the physical velocity components u and v.

For a typical test the amount of CPU time required on a MicroVax II computer machine was 10 884 s. All test cases were carried out with single-precision accuracy.

Table I shows the flowchart for the calculation of the unsteady two-dimensional flow.

6. COMPUTATIONAL RESULTS AND DISCUSSION

6.1. WES tests (1D flow)

The validity of the proposed computational technique was first tested using 1D flood flow data. A rectangular wooden flume lined with plastic-coated plywood, 122 m long and 1·22 m wide, with a bottom slope $S_{0x}=0{\cdot}005$ was used in the experiments.[19] The model dam was placed at mid-section, impounding water to a depth of 0·3048 m. Experiments were carried out using smooth ($n=0{\cdot}009$) and rough ($n=0{\cdot}050$) Manning flow resistance coefficients.

6.1.1. Comparison with an inviscid solution (characteristics method). The method of characteristics was used by Hunt[17] to obtain the dam-break flood inviscid solution on a sloping channel that was initially dry. The calculated solution was tested against the experimental resuls (WES tests). Comparisons of calculated depth hydrographs between the current method and the method of characteristics at three different stations are shown in Figures 6(a)–6(c). The agreement is satisfactory. The time at which the wave tip reaches station $x=7{\cdot}62$ m (Figure 6(c)) is well predicted. Similarly, the predicted time at which motion begins in the reservoir is in good agreement with the characteristics solution (Figure 6(a)). Notice that although a two-dimensional algorithm is incorporated, one-dimensional results are sought.

6.1.2. Comparison with experimental data and MacCormack's numerical solution. Figures 7(a)–7(c) show comparisons of depth hydrographs predicted by the current method with

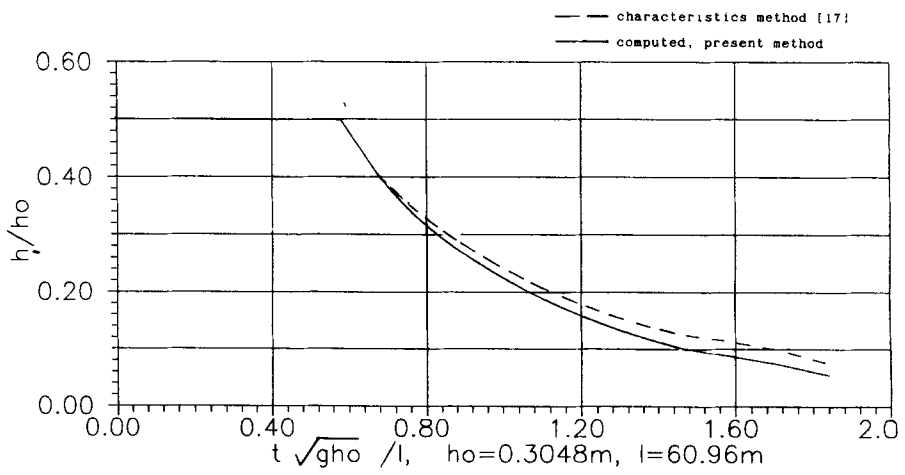

Figure 6(a). Comparison between predicted and characteristics method solution stage hydrographs for WES test; $n=0{\cdot}0$, $S_{0x}=0{\cdot}005$, $h_1=0{\cdot}3048$ m, station $x=-30{\cdot}5$ m

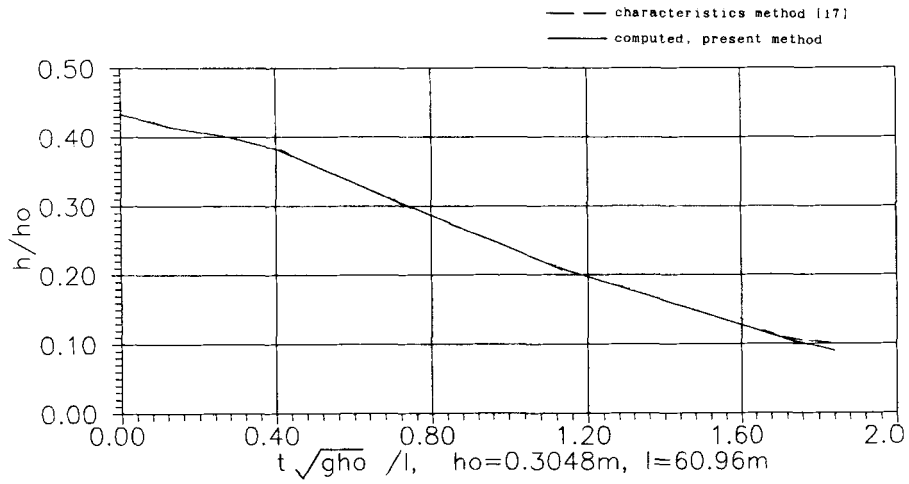

Figure 6(b). Comparison between predicted and characteristics method solution stage hydrographs for WES test; $n=0{\cdot}0$, $S_{0x}=0{\cdot}005$, $h_1=0{\cdot}3048$ m, station $x=0{\cdot}0$ m

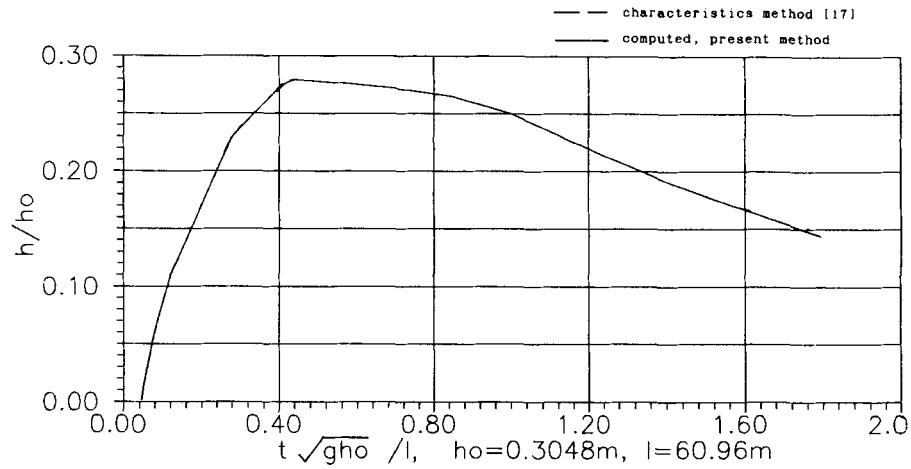

Figure 6(c). Comparison between predicted and characteristics method solution stage hydrographs for WES test; $n=0{\cdot}0$, $S_{0x}=0{\cdot}005$, $h_1=0{\cdot}3048$ m, station $x=7{\cdot}62$ m

measured data as well as with predictions derived from the application of the well-known MacCormack numerical scheme.[8,18] The applied MacCormack scheme is the explicit two-step predictor–corrector numerical technique, which is well suited for flows with abrupt changes of flow quantities. All the above figures refer to low flow resistance ($n=0{\cdot}009$). Again the comparison between predictions and measurements is considered to be satisfactory, although some differences between theory and measurements are appearing at station $x=24{\cdot}4$ m (Figure 7(c)). Finally, Figures 8(a)–8(c) show the comparisons for high flow resistance ($n=0{\cdot}050$) at the same stations, i.e. $x=-30{\cdot}5$, $0{\cdot}0$ and $24{\cdot}4$ m. The agreement between theory and measurements remains equally satisfactory for this high-flow-resistance test case.

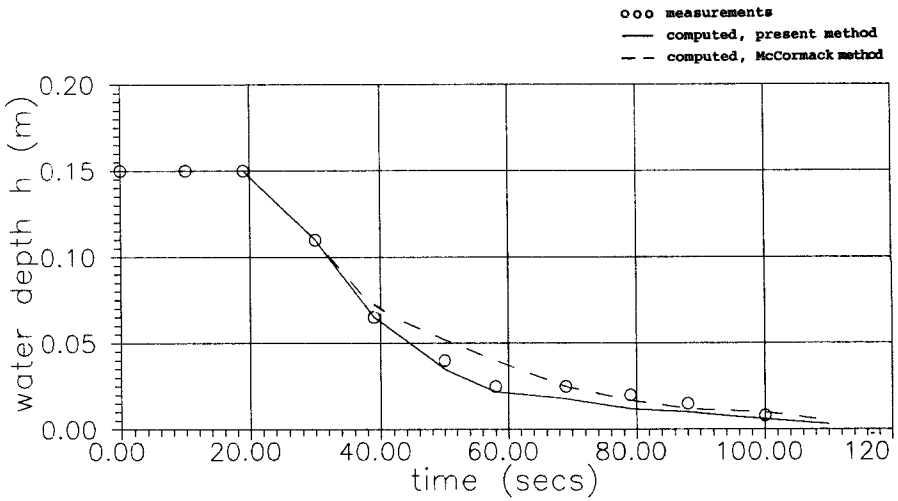

Figure 7(a). Comparison between predicted, MacCormack's numerical solution and measured stage hydrographs for WES test; low-flow-resistance condition $n=0{\cdot}009$, $S_{0x}=0{\cdot}005$, $h_1=0{\cdot}3048$ m, station $x=-30{\cdot}5$ m

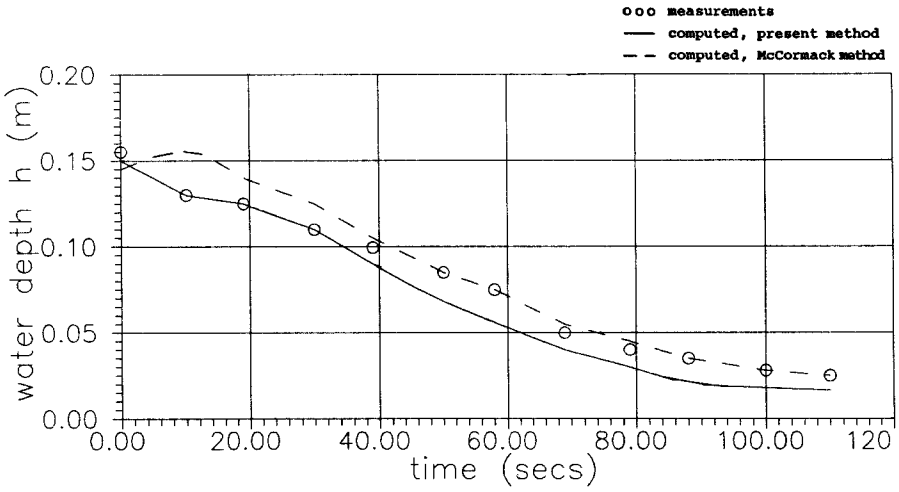

Figure 7(b). Comparison between predicted, MacCormack's numerical solution and measured stage hydrographs for WES test; low-flow-resistance condition $n=0{\cdot}009$, $S_{0x}=0{\cdot}005$, $h_1=0{\cdot}3048$ m, station $x=0{\cdot}0$ m

6.2. Thrace University tests (2D flow)

The movement on a dry bed of a two-dimensional flood wave resulting from a dam-break was experimentally investigated by Bellos[10] and Bellos *et al.*[9] A converging–diverging flume configuration with a hypothetical dam located right at the throat of the flume was tested. Measured water depths with respect to time were obtained at various cross-sections along the centreline of the channel. The tested flume geometry is shown in Figure 9. The physical problem under

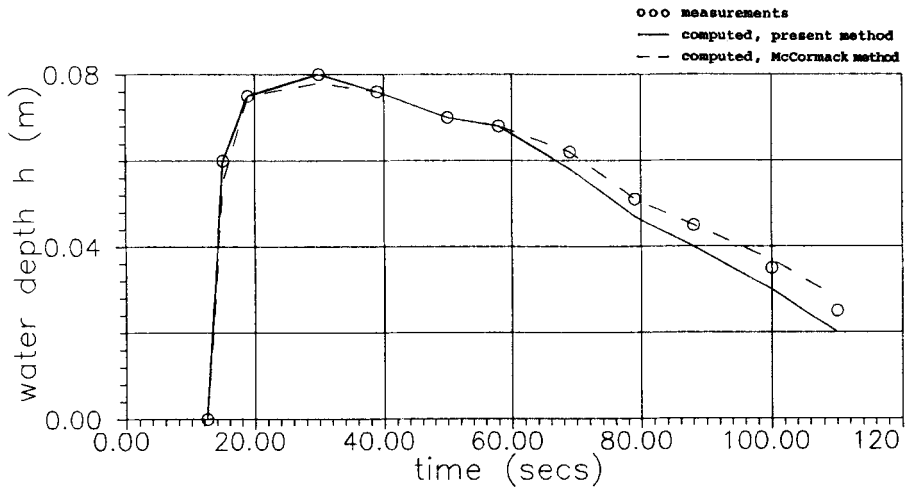

Figure 7(c). Comparison between predicted, MacCormack's numerical solution and measured stage hydrographs for WES test; low-flow-resistance condition $n=0{\cdot}009$, $S_{0x}=0{\cdot}005$, $h_1=0{\cdot}3048$ m, station $x=24{\cdot}4$ m

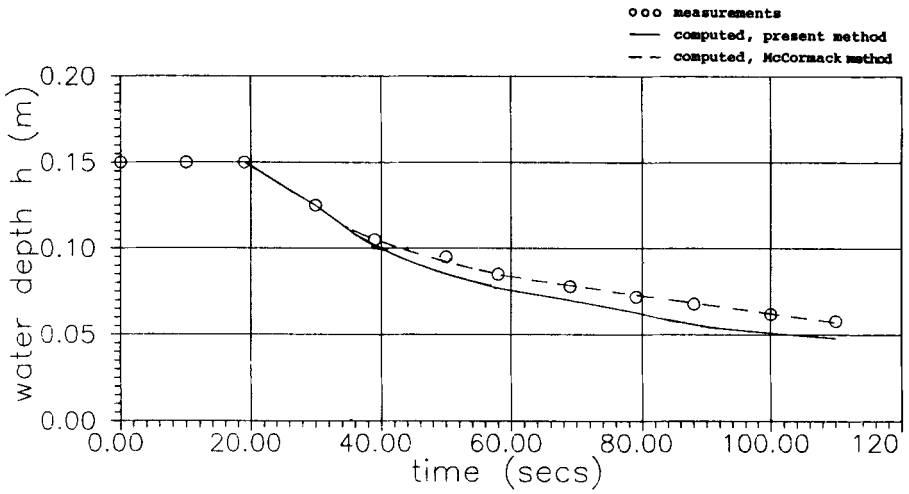

Figure 8(a). Comparison between predicted, MacCormack's numerical solution and measured stage hydrographs for WES test 1·2; high-flow-resistance condition $n=0{\cdot}050$, $S_{0x}=0{\cdot}005$, $h_1=0{\cdot}3048$ m, station $x=-30{\cdot}5$ m

consideration is of mixed subcritical–supercritical type of flow with abrupt changes of the physical quantities (depth, velocities).

6.2.1. Comparison with experiments. Measured stage hydrographs at various locations along the centreline of the rectangular cross-section flume are compared with current method predictions. These hydrographs refer to positions $x=-8{\cdot}5$, 0·0, 5·0 and 10·0 m and are shown in

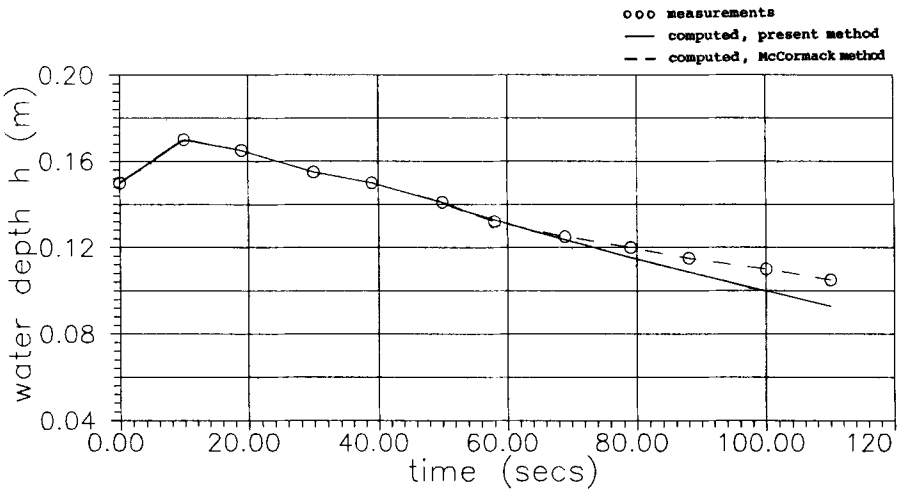

Figure 8(b). Comparison between predicted, MacCormack's numerical solution and measured stage hydrographs for WES test 1·2; high-flow-resistance condition $n=0{\cdot}050$, $S_{0x}=0{\cdot}005$, $h_1=0{\cdot}3048$ m, station $x=0{\cdot}0$ m

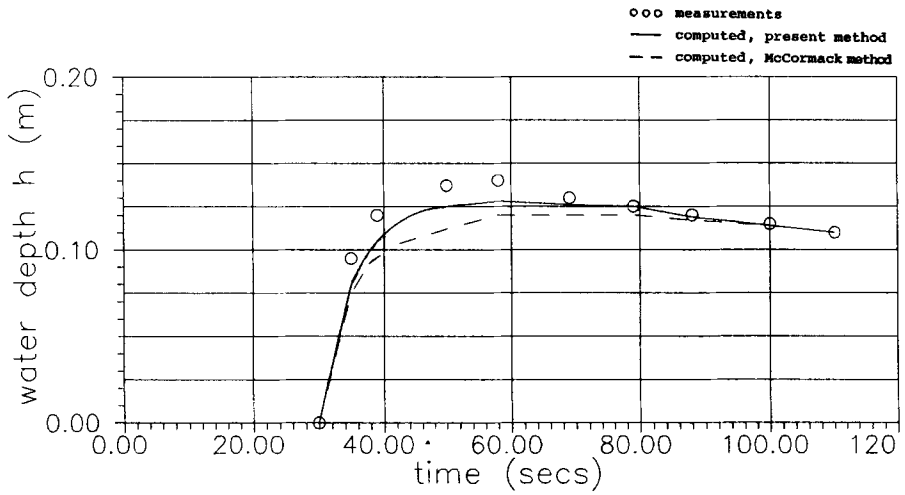

Figure 8(c). Comparison between predicted, MacCormack's numerical solution and measured stage hydrographs for WES test 1·2; high-flow-resistance condition $n=0{\cdot}050$, $S_{0x}=0{\cdot}005$, $h_1=0{\cdot}3048$ m, station $x=24{\cdot}4$ m

Figures 10(a)–10(d) respectively. The bed slopes S_{0x} and S_{0y} are both zero while the initial upstream (from the dam-site) water depth h_1 was equal to 30·0 and 15·0 cm. When the bed slope S_{0x} is increased to 0·010 while S_{0y} remains zero, the corresponding stage hydrographs are as shown in Figures 11(a)–11(d).

In all above figures the two-dimensional flow effects are considered to result from the converging–diverging flume geometry. These effects appear as bumps in nearly all these figures.

No	x [m]	y [m]	No	x [m]	y [m]	No	x [m]	y [m]	No	x [m]	y [m]
1	-8.50	1.40	9	0.00	0.60	17	4.00	0.99	25	8.00	1.40
2	-3.50	1.40	10	0.50	0.61	18	4.50	1.08	26	12.70	1.40
3	-3.00	1.22	11	1.00	0.62	19	5.00	1.15			
4	-2,50	1.05	12	1.50	0.64	20	5.50	1.24			
5	-2.00	0.90	13	2.00	0.68	21	6.00	1.28			
6	-1.50	0.77	14	2.50	0.75	22	6.50	1.33			
7	-1.00	0.67	15	3.00	0.82	23	7.00	1.37			
8	-0.50	0.62	16	3.50	0.91	24	7.50	1.39			

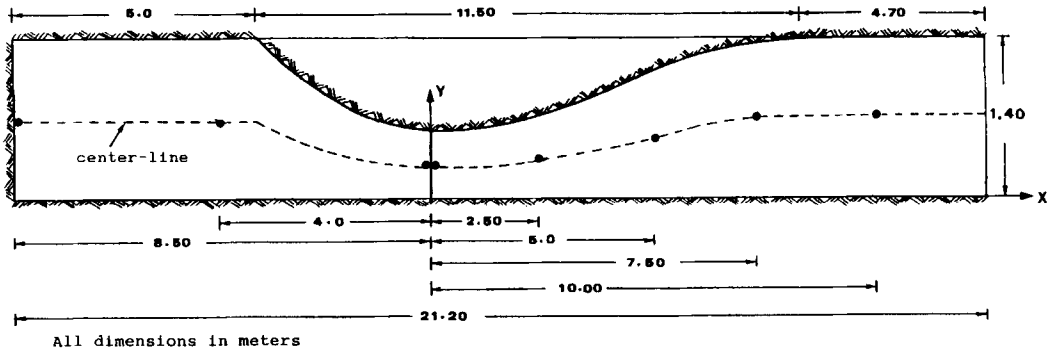

Figure 9. Schematic diagram of tested flume geometry (2D flow)

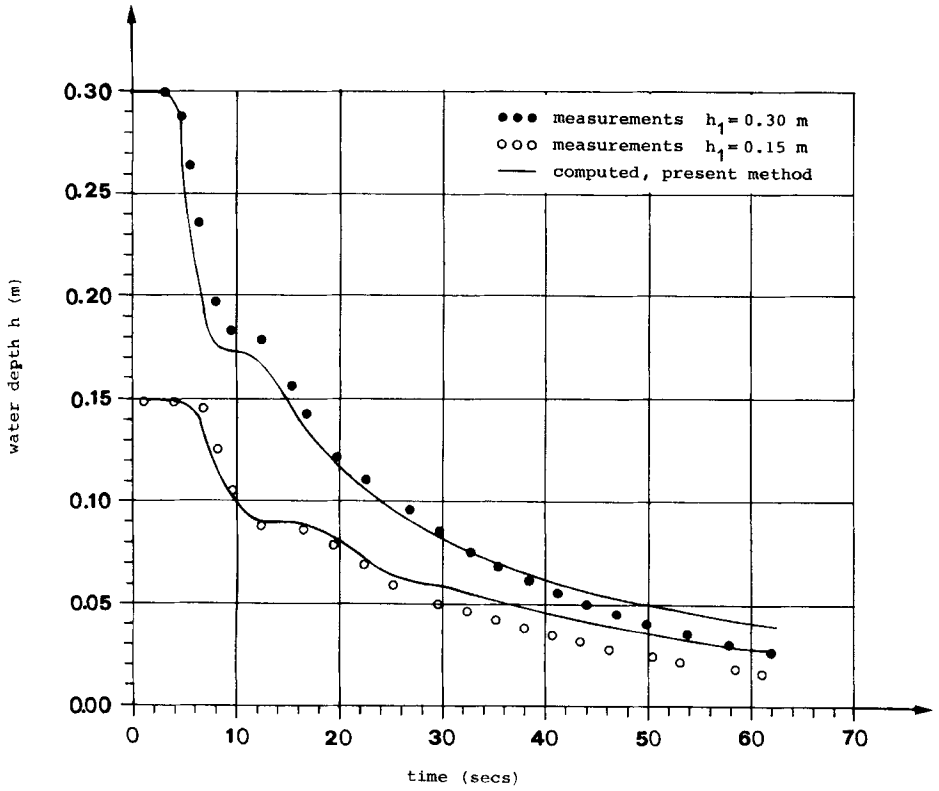

Figure 10(a). Comparison between predicted and measured stage hydrographs for Thrace University test flume; $S_{0x} = 0{\cdot}0$, $S_{0y} = 0{\cdot}0$, station $x = -8{\cdot}5$ m

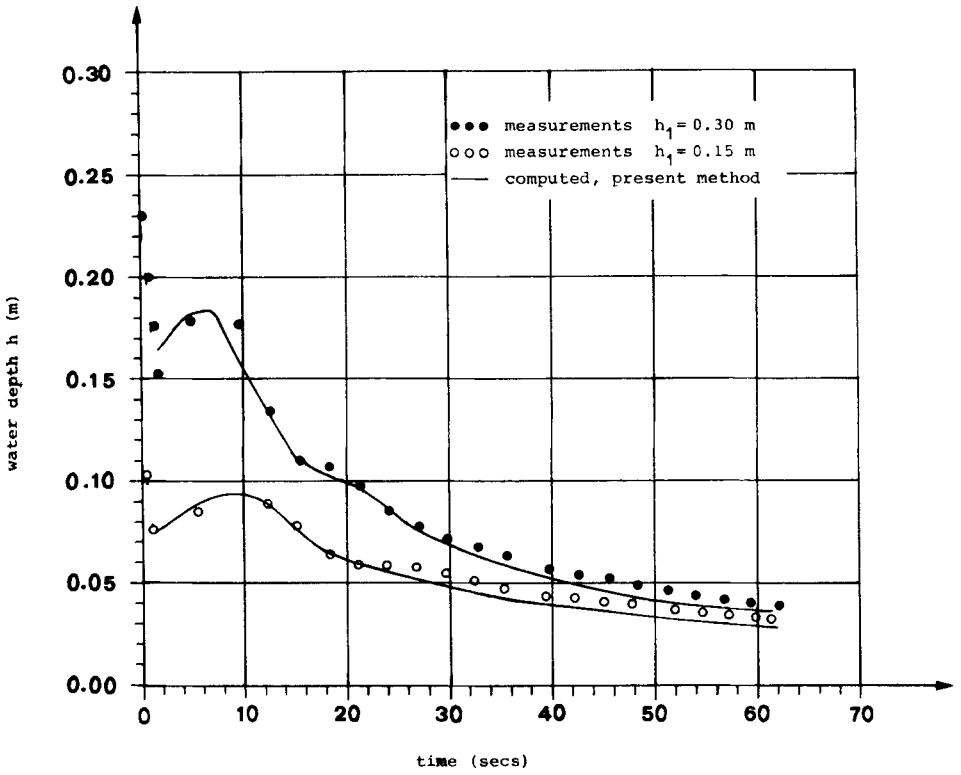

Figure 10(b). Comparison between predicted and measured stage hydrographs for Thrace University test flume; $S_{0x}=0{\cdot}0$, $S_{0y}=0{\cdot}0$, station $x=0{\cdot}0$ m

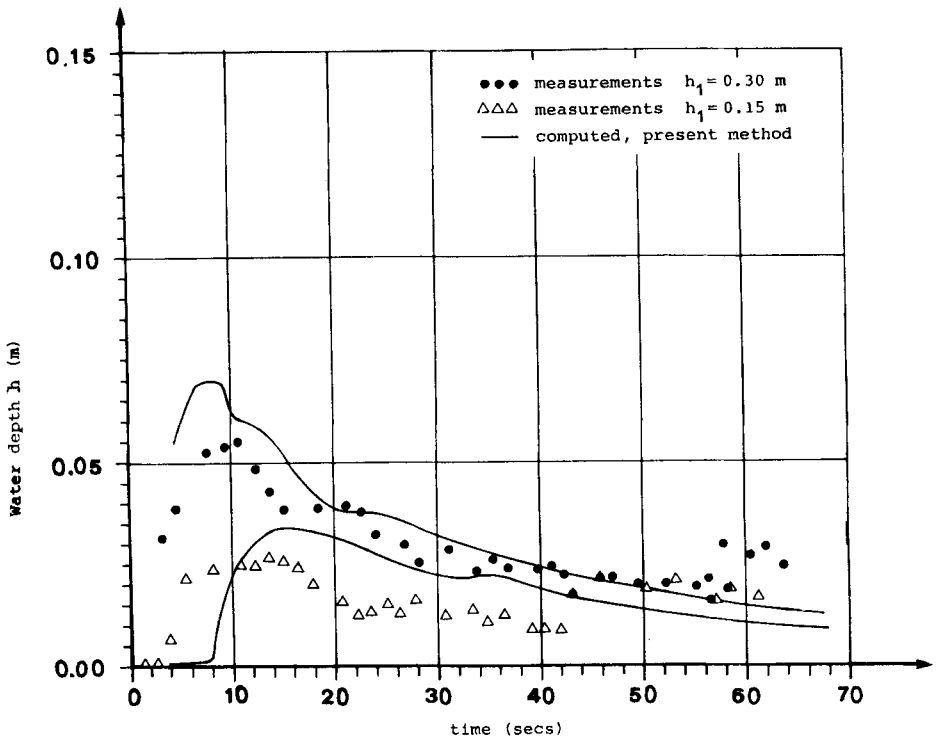

Figure 10(c). Comparison between predicted and measured stage hydrographs for Thrace University test flume; $S_{0x}=0{\cdot}0$, $S_{0y}=0{\cdot}0$, station $x=5{\cdot}0$ m

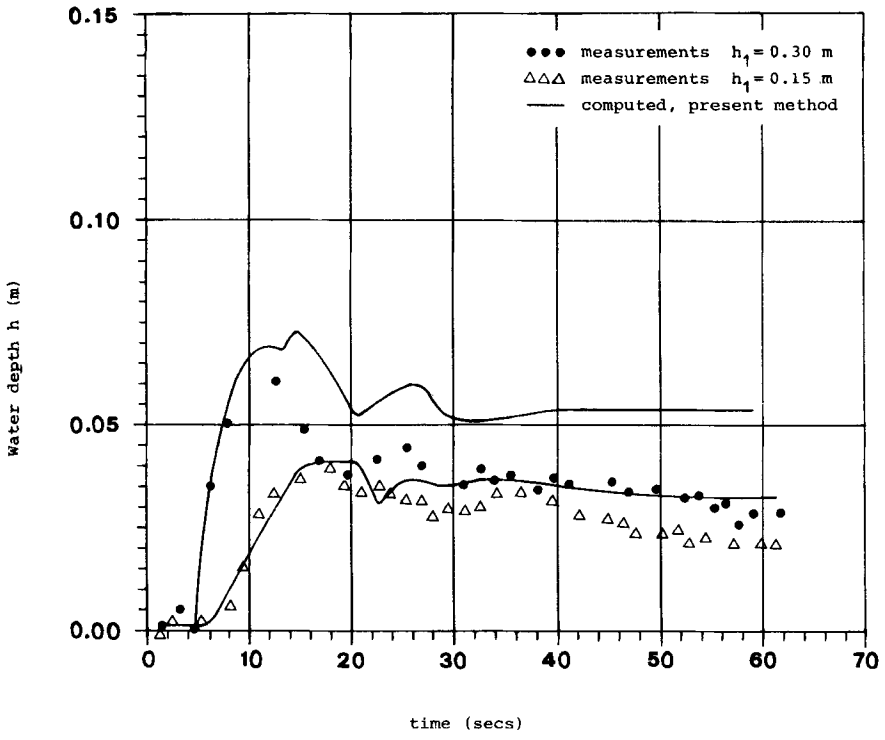

Figure 10(d). Comparison between predicted and measured stage hydrographs for Thrace University test flume; $S_{0x}=0{\cdot}0$, $S_{0y}=0{\cdot}0$, station $x=10{\cdot}0$ m

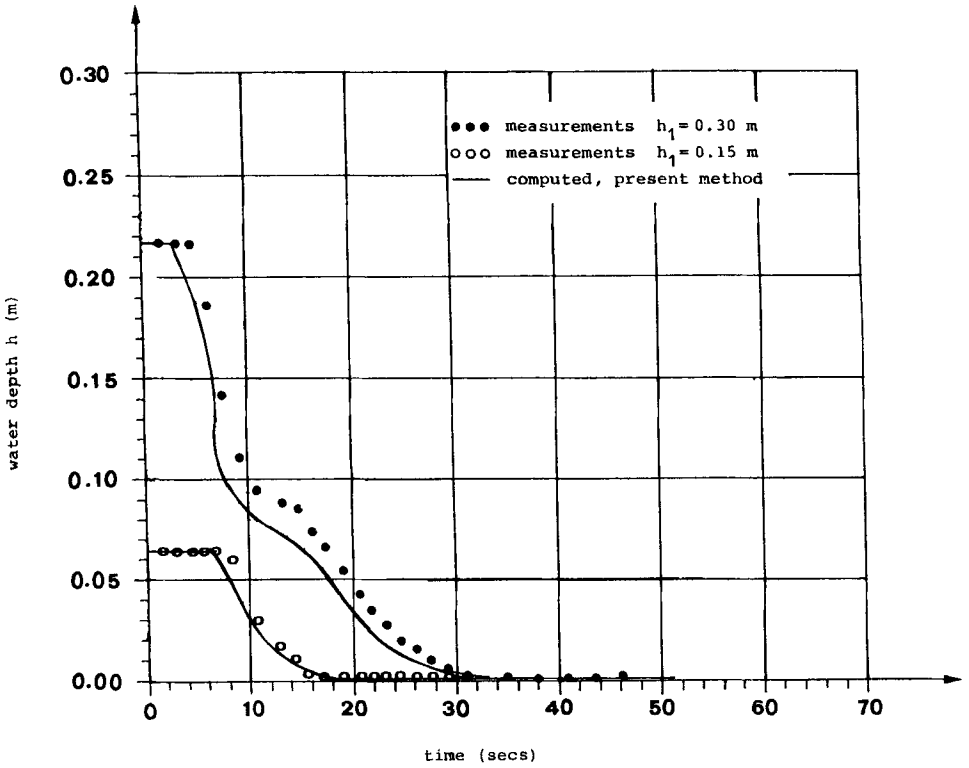

Figure 11(a). Comparison between predicted and measured stage hydrographs for Thrace University test flume; $S_{0x}=0{\cdot}010$, $S_{0y}=0{\cdot}0$, station $x=-8{\cdot}5$ m

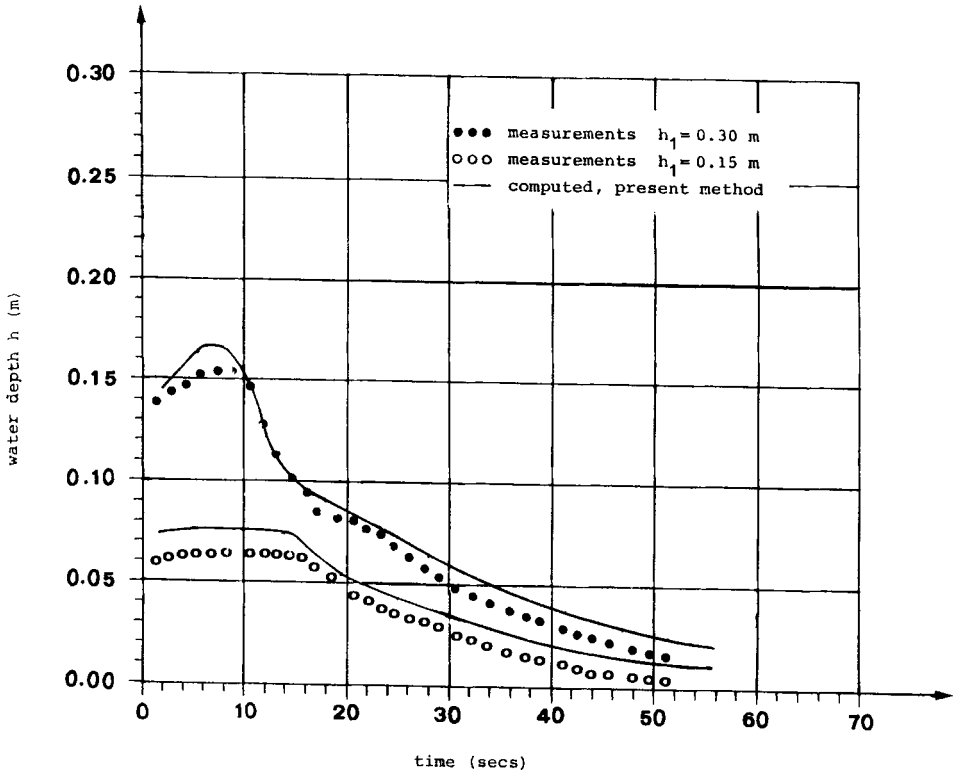

Figure 11(b). Comparison between predicted and measured stage hydrographs for Thrace *University test* flume; $S_{0x}=0{\cdot}010$, $S_{0y}=0{\cdot}0$, station $x=0{\cdot}0$ m

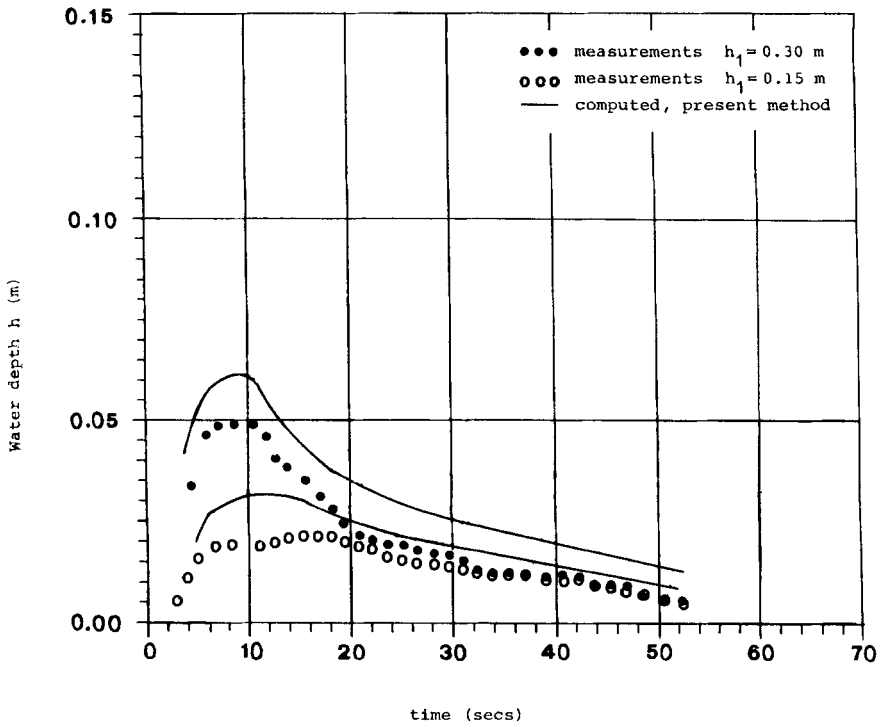

Figure 11(c). Comparison between predicted and measured stage hydrographs for Thrace University test flume; $S_{0x}=0{\cdot}010$, $S_{0y}=0{\cdot}0$, station $x=5{\cdot}0$ m

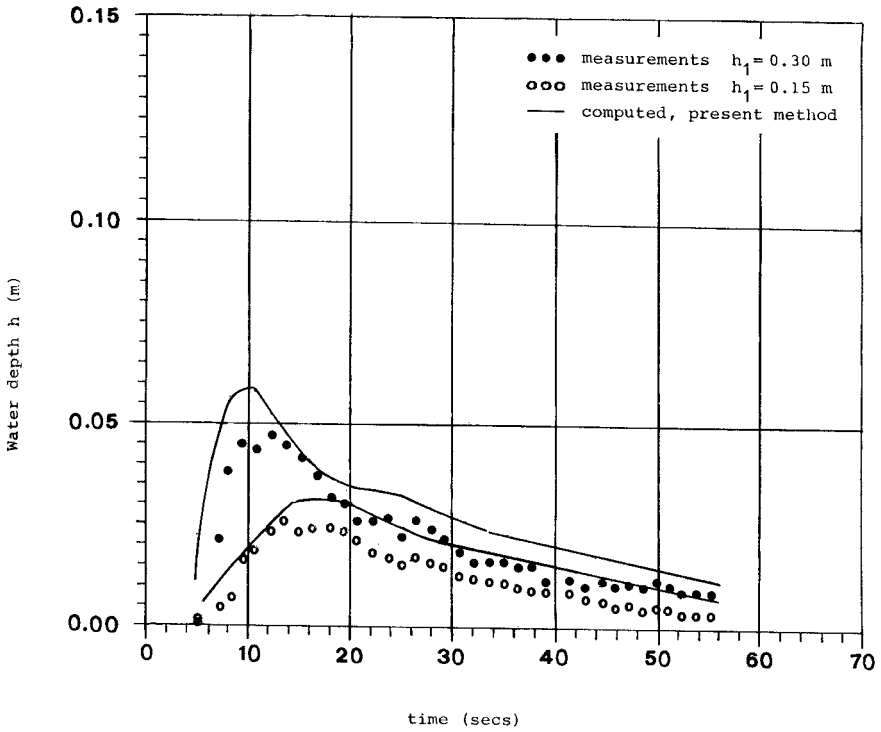

Figure 11(d). Comparison between predicted and measured stage hydrographs for Thrace University test flume; $S_{0x} = 0{\cdot}010$, $S_{0y} = 0{\cdot}0$, station $x = 10{\cdot}0$ m

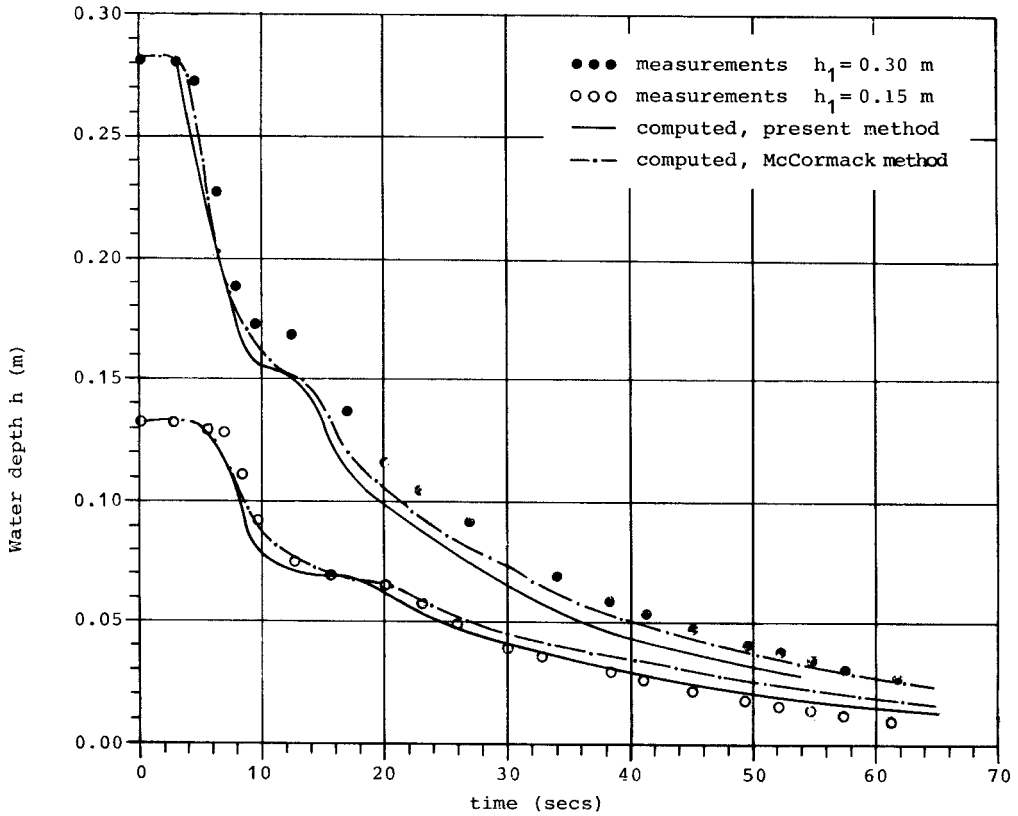

Figure 12(a). Comparison between predicted, MacCormack's numerical solution and measured stage hydrographs for Thrace University test flume; $S_{0x} = 0{\cdot}002$, $S_{0y} = 0{\cdot}0$, station $x = -8{\cdot}5$ m

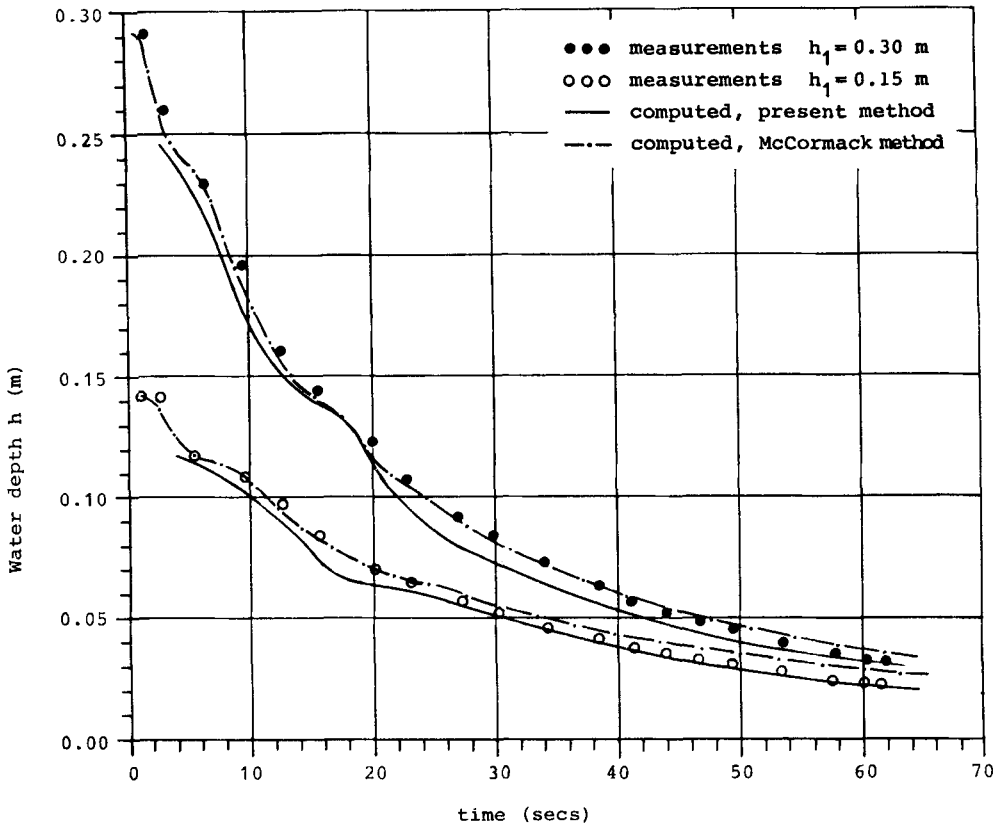

Figure 12(b). Comparison between predicted, MacCormack's numerical solution and measured stage hydrographs for Thrace University test flume; $S_{0x} = 0{\cdot}002$, $S_{0y} = 0{\cdot}0$, station $x = -4{\cdot}0$ m

The Manning flow friction coefficient n was set equal to 0·012, a value which closely approximates the glass–steel material of the tested flume. However, near the dam-site region this value was doubled so as to include the possible interaction of the gate sliding mechanism with the flow. A 13×49 computational grid was used in order to achieve the desired flow accuracy. The utilization of a denser computational grid did not substantially alter the predicted results. The time step Δt was set to 0·03 s, while the total duration of a typical experiment was about 70 s. Within each time step the number of iterations to achieve solution was equal to three in nearly all applied upstream water depths. From all the above figures it is evident that the comparison between measured and computed data is rather satisfactory. The two-dimensional flow effects are also predicted by the proposed method.

6.2.2. Comparison with MacCormack's explicit numerical solution. To validate the predicted results, it was decided to compare them with the previously developed[8] numerical algorithm which applies the two-step explicit scheme developed by MacCormack. All these predictions were plotted against the available experimental data. Figures 12(a)–12(e) show comparisons of the stage hydrographs for the testing flume at various stations when $S_{0x} = 0{\cdot}002$, $S_{0y} = 0{\cdot}0$ and the

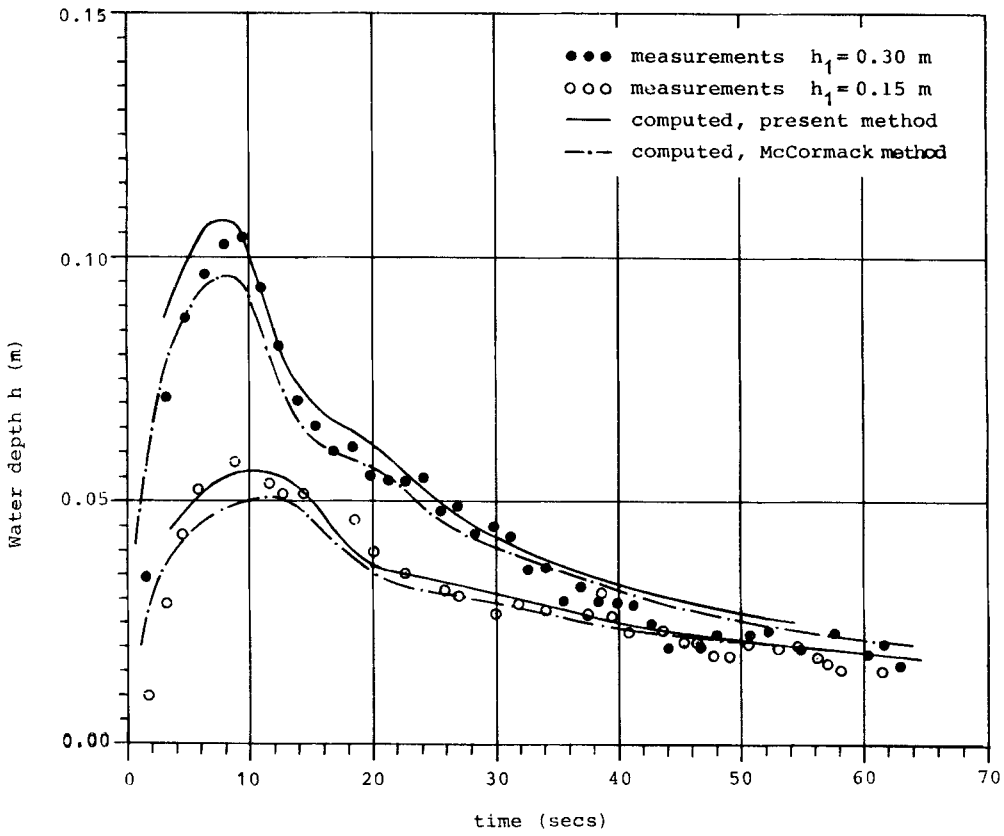

Figure 12(c). Comparison between predicted, MacCormack's numerical solution and measured stage hydrographs for Thrace University test flume; $S_{0x} = 0{\cdot}002$, $S_{0y} = 0{\cdot}0$, station $x = 2{\cdot}5$ m

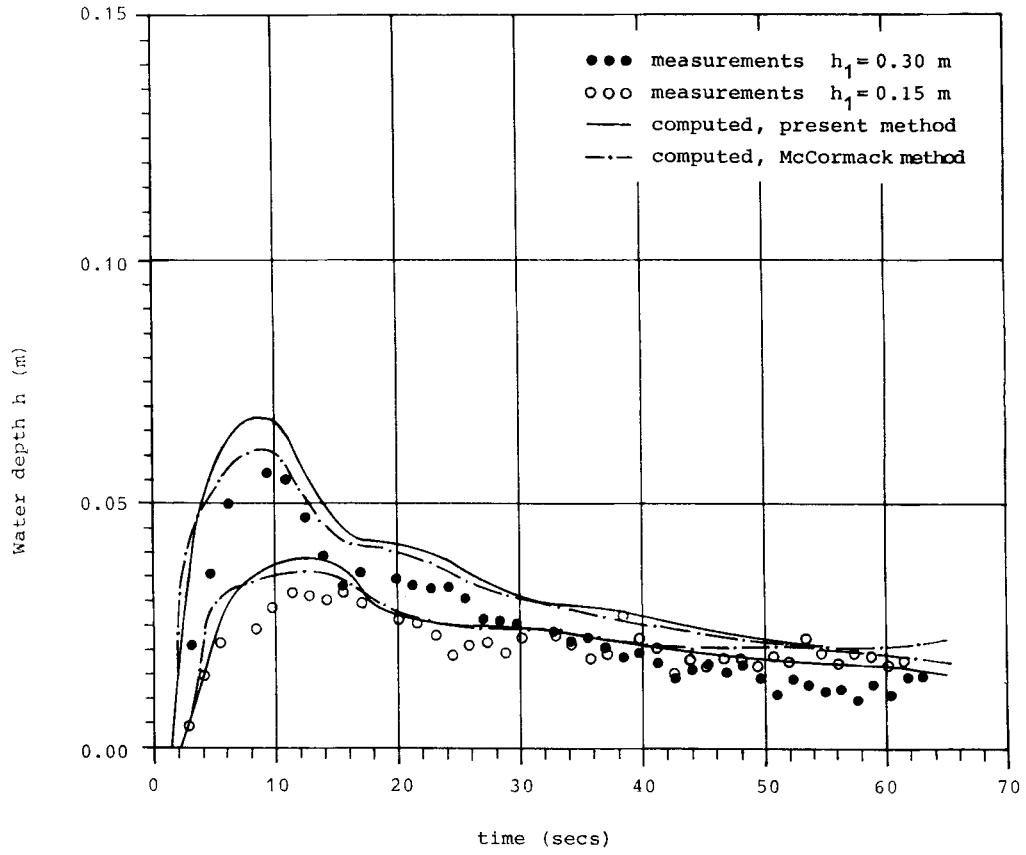

Figure 12(d). Comparison between predicted, MacCormack's numerical solution and measured stage hydrographs for Thrace University test flume; $S_{0x} = 0{\cdot}002$, $S_{0y} = 0{\cdot}0$, station $x = 5{\cdot}0$ m

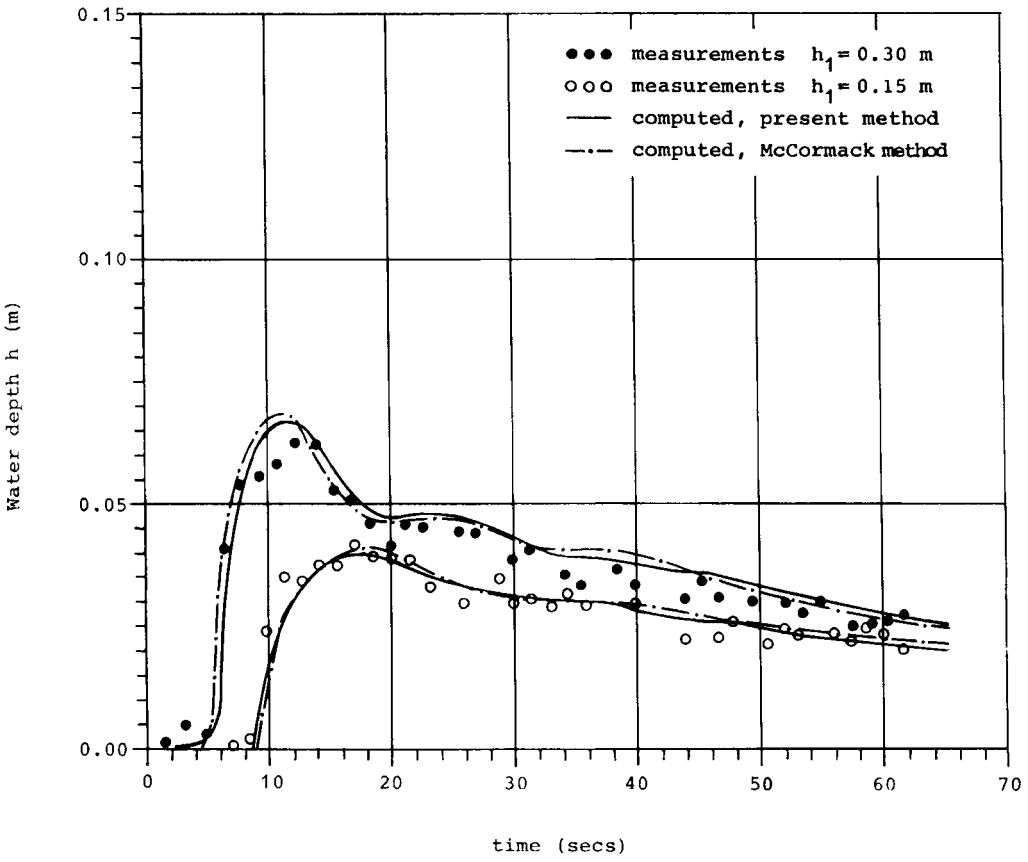

Figure 12(e). Comparison between predicted, MacCormack's numerical solution and measured stage hydrographs for Thrace University test flume; $S_{0x}=0{\cdot}002$, $S_{0y}=0{\cdot}0$, station $x=10{\cdot}0$ m

initial depth at the dam-site $h_1=0{\cdot}30$ and $0{\cdot}15$ m. These comparisons are considered to be satisfactory for both upstream (subcritical) and downstream (supercritical) flow regions. The passing of the flood wave is well predicted. Also, the predictions capture the two-dimensional flow effects of the converging–diverging flume. Note that the predictions tend to agree better with each other than with the measured data. The Manning flow resistance coefficient remains at $0{\cdot}012$, while its value is doubled in the dam-site region. The need to apply an elaborate turbulence model in order to simulate the measured results better is apparent.

When the bottom slope S_{0x} is increased to $0{\cdot}008$ while all the other physical conditions remain the same, the results of the comparisons appear as in Figures 13(a)–13(e). Here again the agreement is satisfactory. The flood routing is faster, as expected, at high bed slopes and this is caused by increased gravitational forces.

6.2.3. Prediction of longitudinal Froude number. The two-dimensional flow behaviour is better seen through the longitudinal Froude number distribution for the straight and curved side walls of the tested flume configuration (see Figure 9). The presented test case (see Figures 14(a)–14(e))

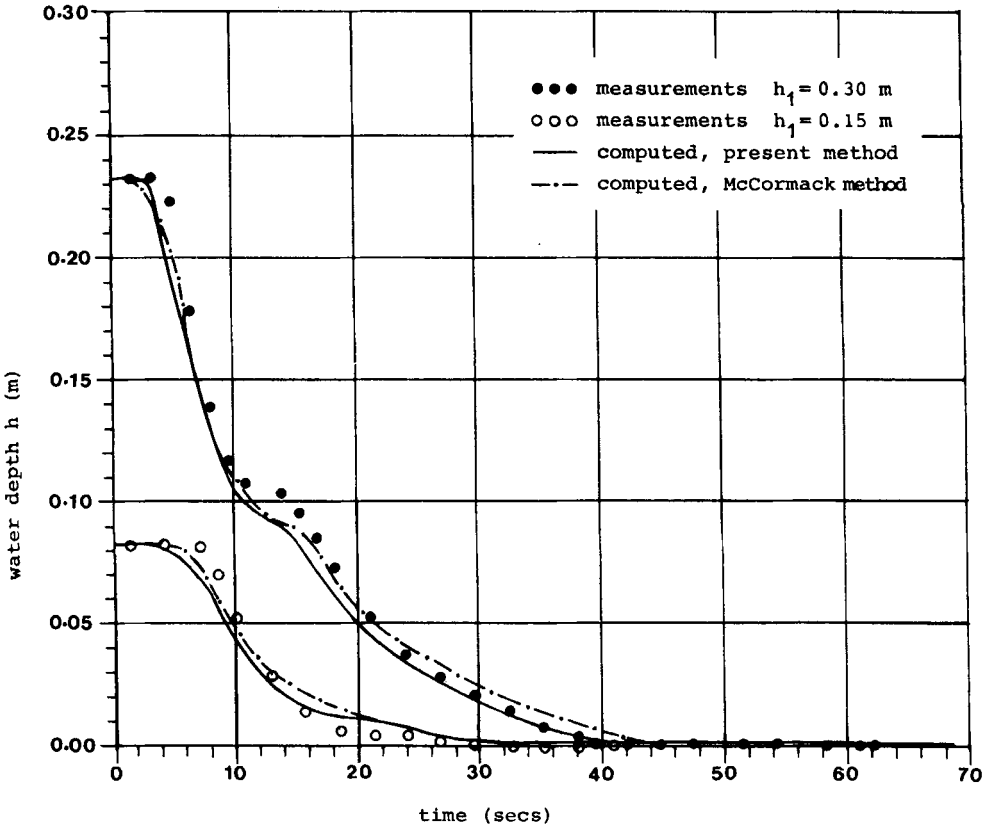

Figure 13(a). Comparison between predicted, MacCormack's numerical solution and measured stage hydrographs for Thrace University test flume; $S_{0x}=0{\cdot}008$, $S_{0y}=0{\cdot}0$, station $x=-8{\cdot}5$ m

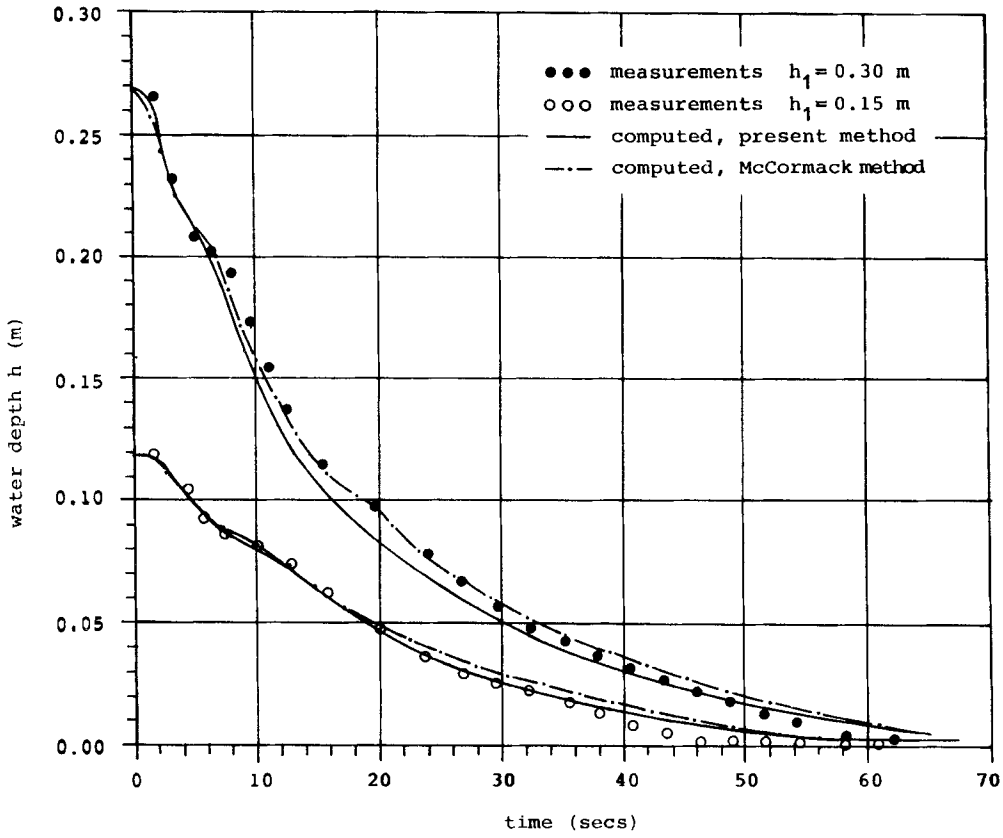

Figure 13(b). Comparison between predicted, MacCormack's numerical solution and measured stage hydrographs for Thrace University test flume; $S_{0x}=0{\cdot}008$, $S_{0y}=0{\cdot}0$, station $x=-4{\cdot}0$ m

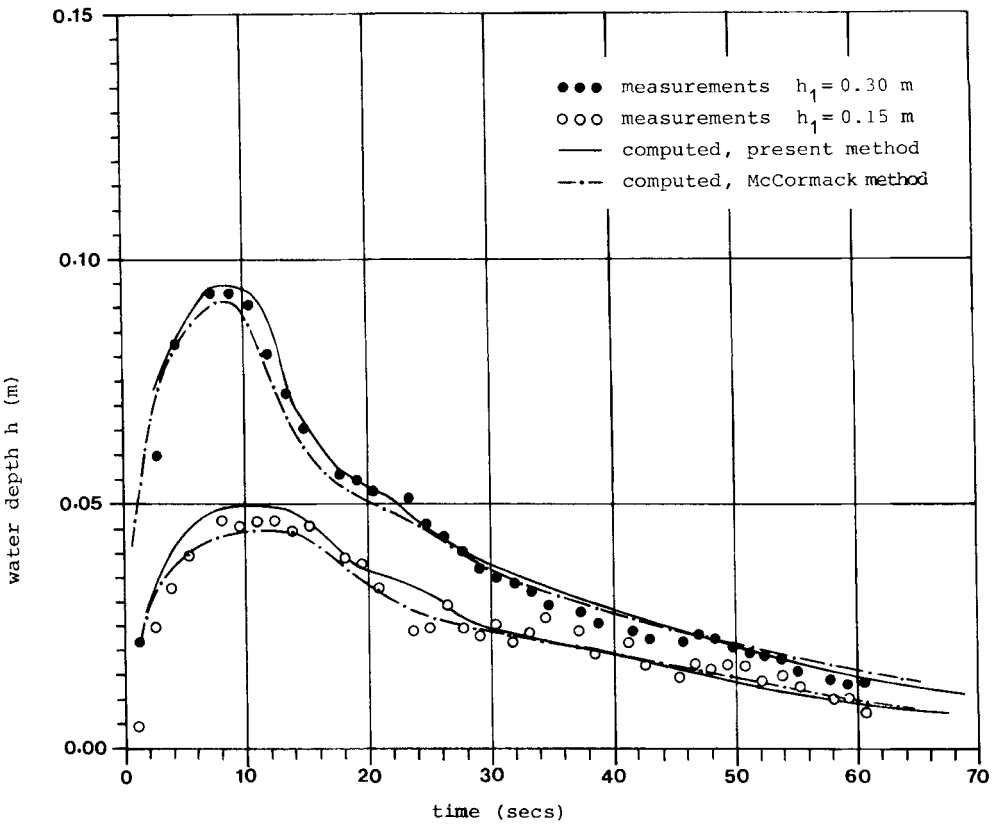

Figure 13(c). Comparison between predicted, MacCormack's numerical solution and measured stage hydrographs for Thrace University test flume; $S_{0x}=0{\cdot}008$, $S_{0y}=0{\cdot}0$, station $x=2{\cdot}5$ m

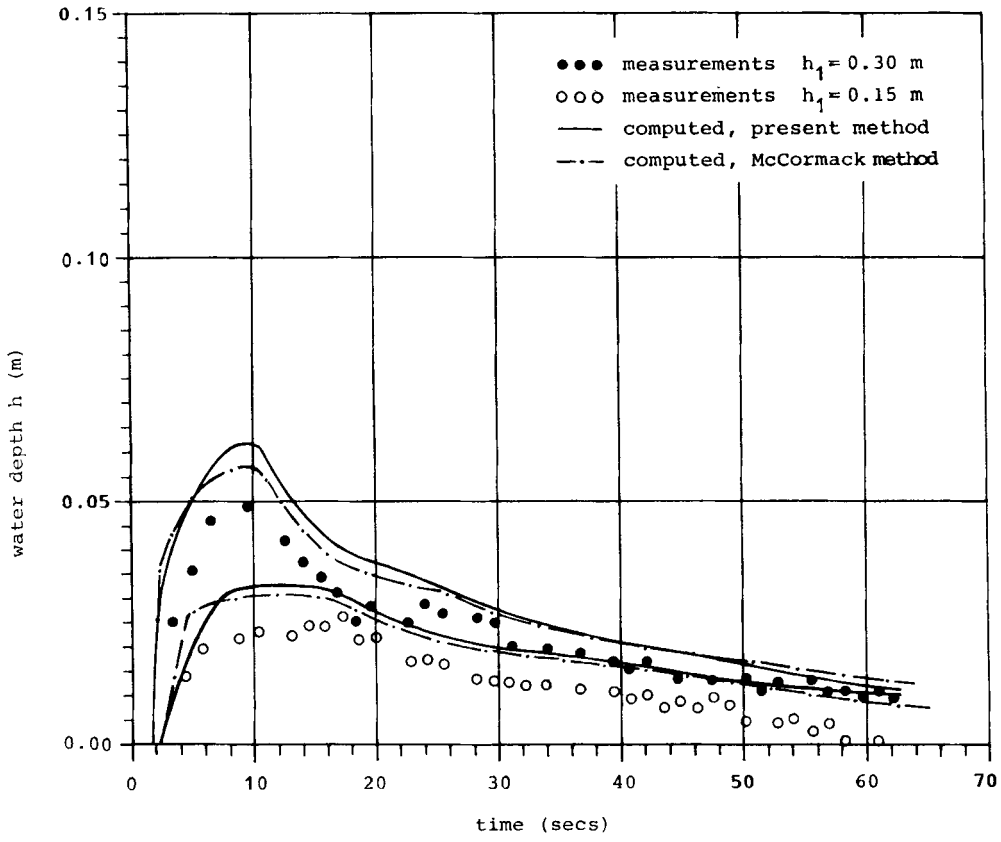

Figure 13(d). Comparison between predicted, MacCormack's numerical solution and measured stage hydrographs for Thrace University test flume; $S_{0x}=0{\cdot}008$, $S_{0y}=0{\cdot}0$, station $x=5{\cdot}0$ m

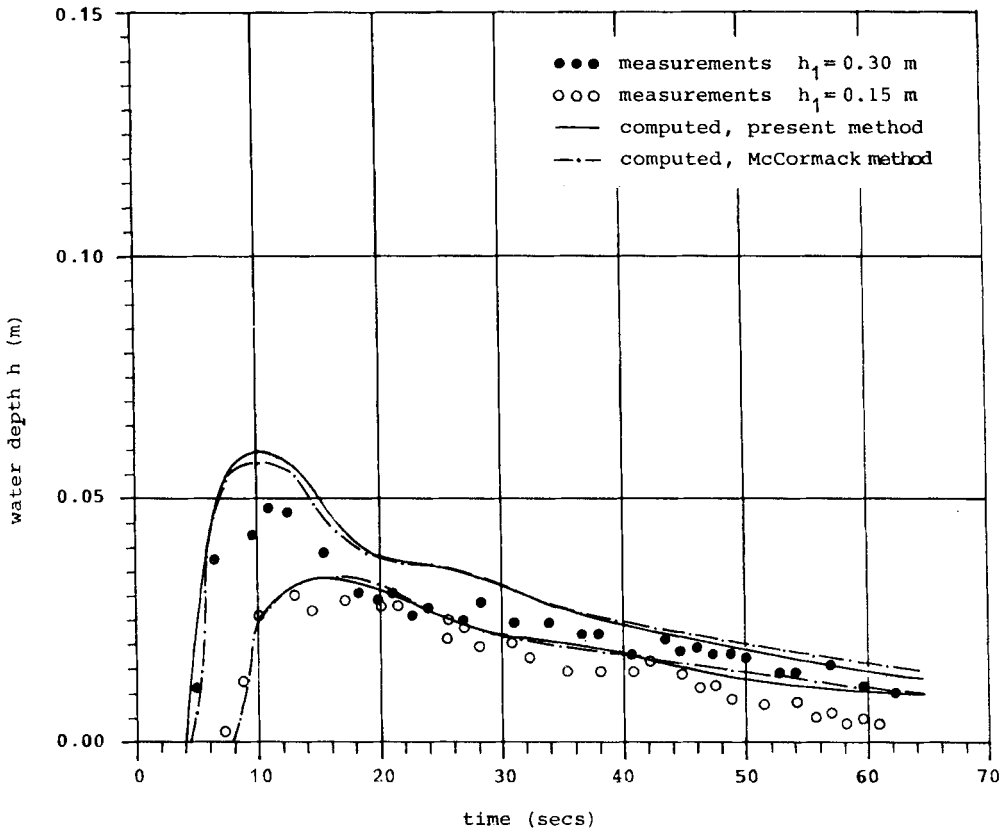

Figure 13(e). Comparison between predicted, MacCormack's numerical solution and measured stage hydrographs for Thrace University test flume; $S_{0x}=0{\cdot}008$, $S_{0y}=0{\cdot}0$, station $x=10{\cdot}0$ m

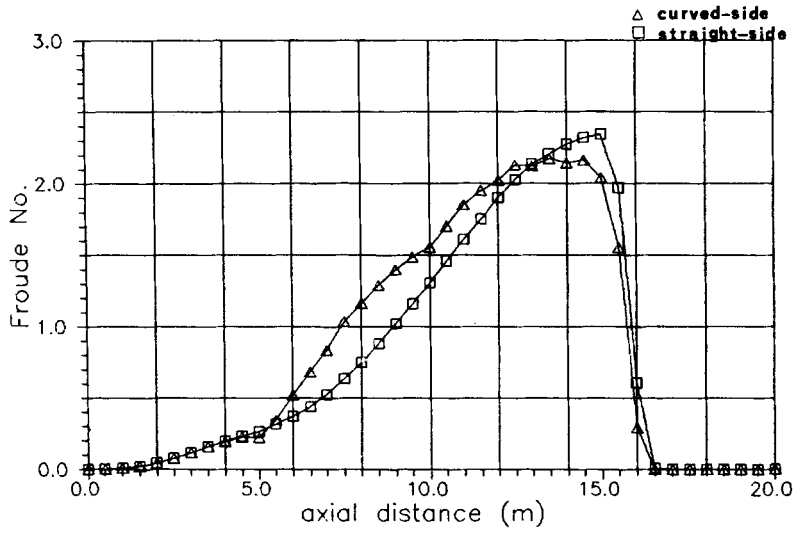

Figure 14(a). Predicted Froude number distribution for Thrace University test flume; $S_{0x}=0{\cdot}0$, $S_{0y}=0{\cdot}0$, $h_1=0{\cdot}30$ m, $t=3{\cdot}439$ s

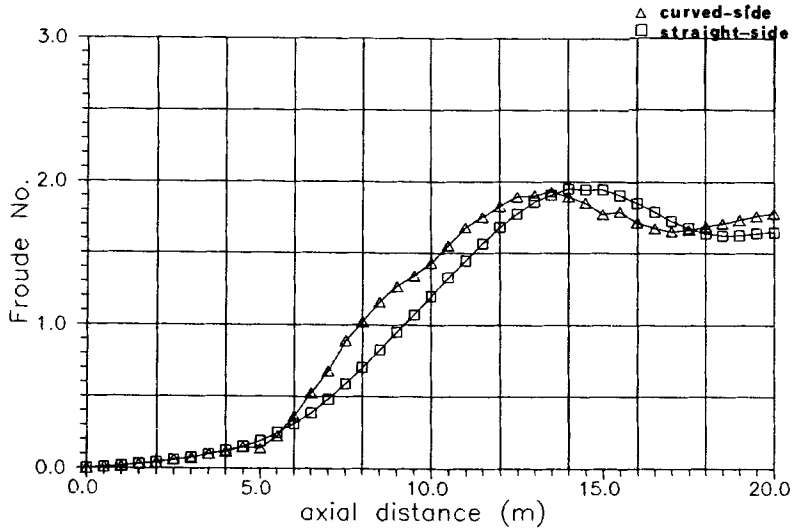

Figure 14(b). Predicted Froude number distribution for Thrace University test flume; $S_{0x}=0{\cdot}0$, $S_{0y}=0{\cdot}0$, $h_1=0{\cdot}30$ m, $t=8{\cdot}598$ s

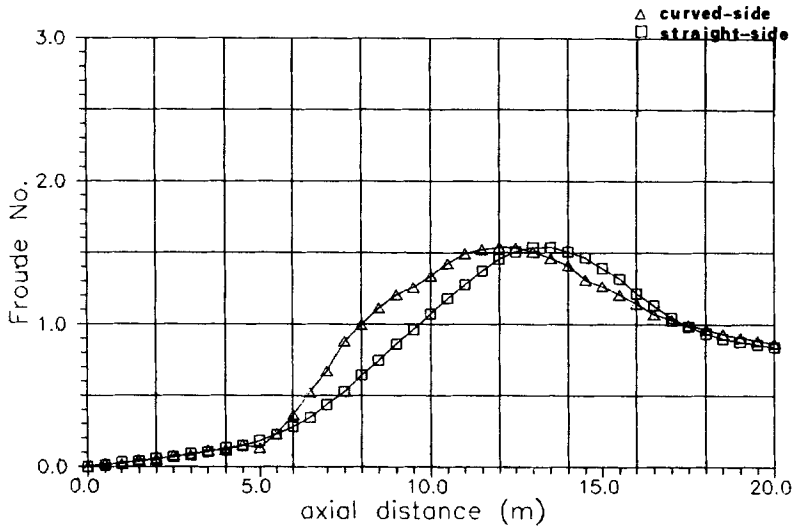

Figure 14(c). Predicted Froude number distribution for Thrace University test flume; $S_{0x}=0{\cdot}0$, $S_{0y}=0{\cdot}0$, $h_1=0{\cdot}30$ m, $t=20{\cdot}664$ s

uses $h_1=0{\cdot}30$ m, $S_{0x}=0{\cdot}0$, $S_{0y}=0{\cdot}0$ and $n=0{\cdot}012$, while dry bed conditions are applied in the downstream region, i.e. $h_2=0{\cdot}0$ m. The dam is located right at the throat of the flume, i.e. 8·5 m from the upstream end of the tested flume. The curved side, for all time levels, yields higher Froude numbers than the straight side for the near-downstream region. However, this trend is

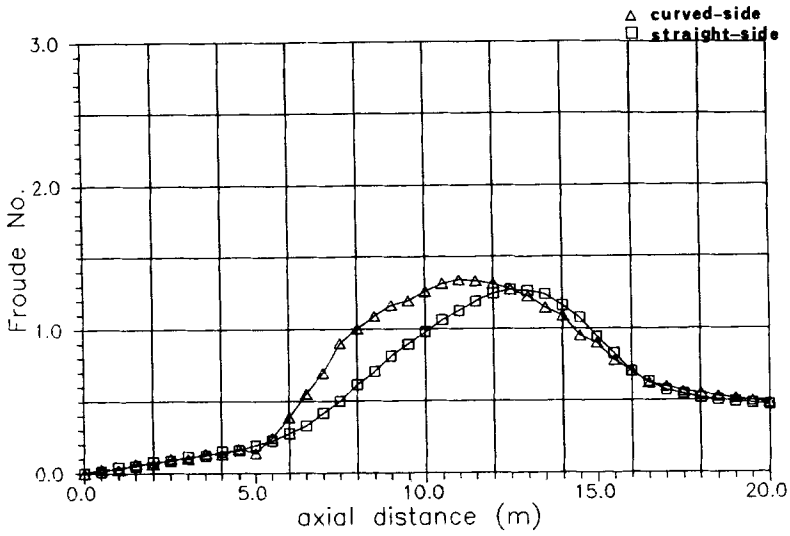

Figure 14(d). Predicted Froude number distribution for Thrace University test flume; $S_{0x}=0{\cdot}0$, $S_{0y}=0{\cdot}0$, $h_1=0{\cdot}30$ m, $t=30{\cdot}982$ s

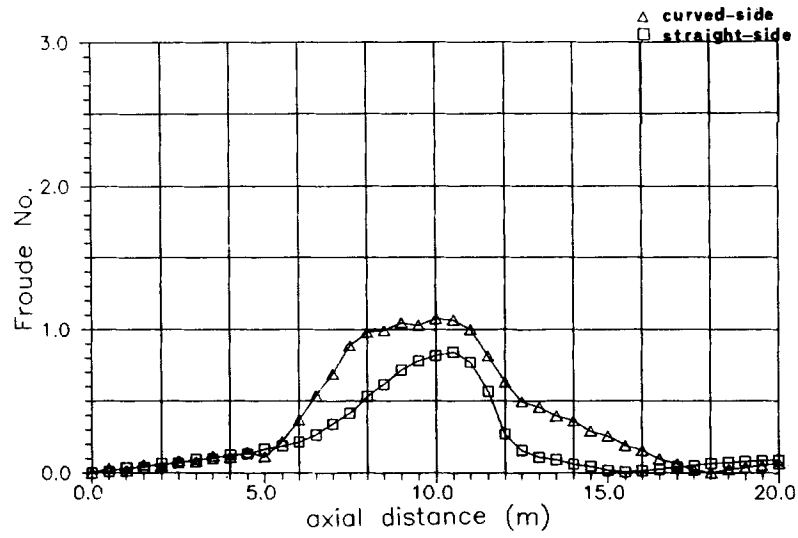

Figure 14(e). Predicted Froude number distribution for Thrace University test flume; $S_{0x}=0{\cdot}0$, $S_{0y}=0{\cdot}0$, $h_1=0{\cdot}30$ m, $t=51{\cdot}645$ s

reversed further downstream where the side walls of the flume are parallel to each other. Of course, high Froude numbers of the order 2·4 appear in the early stages ($t=3{\cdot}439$ s, see Figure 14(a)) of the rupture of the dam. Later on the maximum Froude number is gradually reducing.

7. CONCLUSIONS

An implicit time-marching finite volume numerical scheme was developed and subsequently applied for the solution of the two-dimensional unsteady open channel flow equations written in conservation form. In order to avoid the problems associated with a conventional grid system, a body-fitted non-orthogonal local co-ordinate system was utilized. The proposed numerical technique was applied to determine the stage hydrographs, water surface profiles and velocity components of flood waves resulting from suddenly breached storage dams. The numerical scheme should adequately resolve the resulting mixed subcritical–supercritical flow field. Numerical difficulties as well as diffusion of the wave front arise owing to the very small water depths at the boundaries of the flow field. Thus the numerical code must avoid these unfavourable conseqences. Predictions were compared with an analytical solution (1D flows) as well as with available numerical solutions using MacCormack's two-step explicit scheme and with experimental measurements (2D flows). Agreement between predictions and measurements regarding the wave front advancement and stage hydrographs is considered to be satisfactory. Also, the agreement between the current method predictions and those using an explicit numerical scheme was found to be satisfactory. The method can be expanded to calculate 3D dam-break-induced flows.

REFERENCES

1. T. Xanthopoulos and C. Koutitas, 'Numerical simulation of a two-dimensional flood wave propagation due to dam failure', *J. Hydraul. Res.*, **14**, 321–331 (1976).
2. M. Gallati, G. Braschi, A. DiFillipo and U. Rossi, 'Simulation of the inundation of large areas of complex topography caused by heavy floods', *Proc. Third Int. Conf. on Hydraulic Engineering Software*, Boston, MA, April 1990, pp. 134–147.
3. J. M. Townson and A. H. Al-Salihi, 'Models of dam-break flow in "*R–T*" space', *J. Hydraul. Eng., ASCE*, **115**, (1989).
4. N. D. Katopodes and T. Strelkoff, 'Computing two-dimensional dam-break flood waves', *J. Hydraul. Div., ASCE*, **104**, 1269–1288 (1979).
5. C. Popovska, 'Numerical model for two-dimensional unsteady flow in open channels', *Proc. Third Int. Conf. on Hydraulic Engineering Software*, Boston, MA, April 1990, pp. 149–154.
6. R. Rajar and M. Cetina, 'Two-dimensional dam-break flow in steep curves channels', *Proc. XX Congr. IAHR*, Moscow, 1983, pp. 571–579.
7. D. C. Dammuller, S. M. Bhallamudi and H. M. Chaudhry, 'Modelling of unsteady flow in curved channel', *J. Hydraul. Eng., ASCE*, **115**, 1479–1495 (1989).
8. C. V. Bellos, J. V. Soulis and J. G. Sakkas, 'Computing 2D unsteady open chanel flow by finite-volume metod', *Proc. VII Int. Conf. on Computational Methods in Water Resources*, Boston, MIT, June 1990, pp. 357–362.
9. C. V. Bellos, J. V. Soulis and J. G. Sakkas, 'Open channel flow depth measurements', *Proc. Third Int. Conf. on Hydraulic Engineering Software*, Boston, MIT, April 1990, pp. 263–276.
10. C. V. Bellos, 'Computation of 2-D water movement in open channels', *Ph.D. Thesis*, Democrition University of Thrace, 1990 (in Greek).
11. R. Garcia and R. A. Kawahita, 'Numerical solution of the St. Venant equations with the MacCormack finite-difference scheme', *Int. j. numer. methods fluids*, **6**, 259–274 (1986).
12. R. J. Fenemma and M. H. Chaudhry, 'Implicit methods for two-dimensional unsteady free-surface flows', *J. Hydraul. Res.*, **27**, 321–332 (1989).
13. N. D. Katopodes and C. T. Wu, 'Explicit computation of discontinuous channel flow', *J. Hydraul. Eng., ASCE*, **112**, 456–475 (1986).
14. P. G. Samuels, 'Two-dimensional modelling of flood flows using the finite-element method', *Proc. Int. Conf. on the Hydraulic Aspects of Floods and Flood Control*, BHRA Fluid Engineering, London, 1983, pp. 229–240.
15. A. Di Monaco and P. Molinaro, 'A finite-element two-dimensional model of free surface flows: verification against experimental data for the problem of the emptying of a reservoir due to dam-breaking', *Proc. 1st Int. Conf. on Computer Methods and Water Resources, Vol. 2*, 1988, pp. 301–312.
16. J. V. Soulis, and C. V. Bellos, 'Steady supercritical open channel flow computations', *Proc. 6th Int. Conf. on Numerical Methods in Laminar and Turbulent Flows*, Swansea, July 1989.
17. B. Hunt, 'An inviscid dam-break solution', *J. Hydraul. Res.*, **25**, 313–326 (1987).
18. C. V. Bellos and J. G. Sakkas, '1-D dam-break flood-wave propagation on dry bed', *J. Hydraul. Eng., ASCE*, **113**, 1510–1524 (1987).

19. WES (Waterways Experiment Station), 'Floods resulting from suddenly breached dams: Report 1, Conditions of minimum resistance; Report 2, Conditions of high resistance', *Miscellaneous Paper 2-374*, U.S. Army Corps of Engineers, Vicksburg, Miss., 1961.
20. A. Ritter, 'Die Fortpflanzung der Wasserwellen', *Z. Verein. Deutsch. Ing.*, **36**, 947–954 (1892).
21. G. Terzidis and T. Strelkoff, 'Computation of open-surges and shocks', *J. Hydraul. Div., Proc. ASCE*, **96**, 2581–2610 (1970).
22. J. V. Soulis and C. V. Bellos, 'Conservation form of fluid dynamics equations in curvilinear coordinate systems', *Tech. Chron. B*, **8**, 69–97 (1988) (in Greek).
23. J. L. Steger, 'Implicit finite-difference simulation of flow about arbitrary two-dimensional geometries', *AIAA J.*, **16**, 679–686 (1978).
24. J. G. Sakkas, 'Flood wave calculation in rivers', *Proc. IInd Panhellenic Hydrological Seminar*, Athens, February 1980, pp. 313–324 (in Greek).